Defining the role of Xin and associated proteins in skeletal muscle health

Michael Akcan

A thesis submitted to the School of Graduate Studies in partial fulfilment of the requirements for the degree Master of Science

McMaster University, Hamilton, ON, Canada, Michael Akcan, July 2021

Acknowledgements

Thank you, to my supervisor Dr. Thomas Hawke for all of your immense support and guidance over the past two years. It was a pleasure to navigate the complexities of studying Xin. You rose to the occasion during unprecedented times and for that I am forever grateful.

Thank you to my committee members Dr. Sandeep Raha and Dr. Gianni Parise for your advice and thoughtful insights. It was always a delight discussing with and learning from you both.

Thank you to all the members of the Hawke and Steinberg lab for making the lab an awesome place to work. Thank you to Irena, Cynthia and Athan, who showed me the ways of the lab and patiently answered all of my questions. Even during those late hours when no one else was around. Thank you to everyone who has worked on the most elusive protein Xin, I am looking forward to what we will discover in the future.

Finally thank you to everyone who has been a part of my journey in academic research since the days of my undergraduate senior thesis. Basic science discovery is remarkable and I'm so glad we could share both the excitement and drama of it together.

Finally, thank you to my family, Ishak, Mehtap, and Stephanie, for always encouraging me and supporting my endeavours.

Table of Contents

Abstract

Xin is a F-actin cytoskeletal remodelling adaptor protein important for skeletal muscle health, including functionality and regeneration. Previous studies from our lab have proposed new roles for Xin based on Xin -/- studies in murine skeletal muscle and satellite cells (SCs). We discovered that Xin also maintained mitochondrial morphology and function and facilitated extracellular Ca^{2+} entry by stabilizing membrane protein channel components. However, these observations lacked a molecular basis, as many of Xin's protein binding partners remain unknown. The main objective of this study was to utilize a Xin overexpression (OE) model to aid in discovering the function of Xin within skeletal muscle and identify new Xin binding partners. While Xin OE had a no discernible effect on myoblast morphological features and F-actin distribution, it significantly hindered differentiation into multi-nucleated myotubes. Time based differentiation assays from Xin OE myoblasts showed myotube lengths were decreased at day 5 (20%; P<.001) and further decreased at day 7 (60%; P<.0001). Xin OE cells displayed an abnormal increase mitochondrial enzyme content (~2.94 fold) and a reduction in myoblast motility (~45%, P <0.05), both which likely contributed to deficits in differentiation. Tracking Xin's subcellular localization, Xin colocalized with mitochondria markers (~71 % Overlap; R^2 0.68) and was present in mitochondria fractionations. Xin co-immunoprecipitated with mitochondrial-associated membrane (MAM) tether proteins: VDAC, Mitofusin 1, and Mitofusin 2. Furthermore, Xin interacted with extracellular calcium entry channels and related proteins such as: Orai1, Stim-1, Junctin, Triadin, and Homer. These results provide further evidence that Xin is a multi-functional protein which regulates mitochondria and cellular calcium entry by directly interacting with MAM tethers and calcium channels. Based on our Xin overexpression

and knockout experiments, these molecular interactions ultimately play a role in myoblast differentiation and maintain contractile and metabolic function within skeletal muscle fibers.

Literature Review

Myocyte cytoskeleton

Introduction to satellite cells

Muscle is one of the largest organs in the human body; accounting for 45% of total body weight, and serving numerous metabolic and anatomical functions.[1] There are 3 primary types of muscle classified as: smooth, cardiac, and skeletal. While each of these muscle types has the common feature of contractility, there are many characteristics which differentiate these muscle types from one another. For example, small, spindle-shaped smooth muscle cells are found in the walls of hollow internal organs (e.g. bladder, gastrointestinal tract, blood vessels) and their slow, rhythmic, involuntary contractions, under control of the autonomic nervous system, propel substances through these hollow organs.[1] Cardiac muscle cells are found in the walls of the heart, and like smooth muscle, have rhythmic contractions under the control of the autonomic nervous system. However, cardiomyocytes are more rectangular in shape, striated in appearance and produce strong contractile force.[2] Skeletal muscle, akin to cardiac myocytes, is striated in appearance and can generate significant force upon contraction. In contrast, contraction of skeletal muscle is voluntary in nature and is controlled by the somatic nervous system.[1] Adult skeletal muscle myocytes consist of long, cylindrical, multinucleated striated cells whose appearance resembles a 'fiber' and thus are frequently referred to as muscle fibers or myofibers. Skeletal muscle fibers arise during embryonic development from the fusion of approximately a hundred small mesodermal cells called myoblasts.[1] Due to this cellular fusion,

each mature skeletal muscle fiber is therefore multi-nucleated. Upon cell fusion, the nuclei of the myofiber undergoes changes which render it post-mitotic, unable to undergo future rounds of cell division[3] Thus, the number of skeletal muscle fibers is set before you are born. However, a small population of myocyte progenitors known as satellite cells (SCs) persist in adulthood which retain their cell division and differentiation ability. SCs lie in close apposition to a myofiber underneath the basal lamina surrounding the myofiber.[4] These cells are normally quiescent in uninjured muscle but can activate and proliferate upon stimulus such as muscle injury. Upon injury, active immune cells invade the injured site and secrete growth factors which help regulate the activation, proliferation and fusion of SCs.[5] These factors are detected by quiescent SCs which then migrate to the site of injury. This niche exposes them to cytokines and growth factors, whereby they proliferate in order to provide enough cells for proper muscle repair and subsequently, differentiate into muscle cells.[1] Muscle cell differentiation is a complex, multi-phase process involving a variety of cellular machineries and culminating in the merger of plasma membranes. Cell culture studies from C2C12 mouse muscle cell lines demonstrate multinucleated myotubes form from myoblasts in a series of steps. Upon activation, myoblasts turn into slightly elongated myocytes which migrate, adhere, and then fuse to one another to form small nascent myotubes.[6] Satellite cells are characterized by the expression of the Pax7 transcription factor and they transform into myoblasts due to expression of the myogenic factors MyoD and Myf5.[4] Nascent myotubes then further fuse with additional myocytes or with other myotubes to generate mature myotubes. Mature differentiation is characterized by the downregulation of Pax7 and MyoD, and the upregulation of terminal differentiation markers like the transcription factor, Myogenin, and the contractile protein,

myosin heavy chain.[7] In extremely damaged muscle, the number of new skeletal muscle fibers that can be formed by satellite cells is not enough compensate for damage. Instead, these muscle areas are replaced by fibrous scar tissues.[5] Severe scarring may restrict movement, cause pain, and damage surrounding muscle tissue. However, new studies suggest muscle connective tissue fibrosis is a necessary hallmark of regenerating muscle, and resident fibroblasts regulate satellite cell expansion.[8,7] During regeneration, there is an increase in connective tissue surrounding the damaged area which maintains the structural and functional integrity of regenerating muscle,[9] orients forming myofibers,[8] and sequesters and presents necessary growth factors.[10] However, excessive extracellular matrix can impede mechanical function and hinder muscle regeneration.[11] Thus, fibrosis must be precisely regulated as to not generate deficient or excessive amounts of connective tissue during muscle regeneration. It is clear, the current literature does not fully understand the biochemical processes by which satellite cells repopulate and regenerate damaged fibers. This knowledge is vital to understand

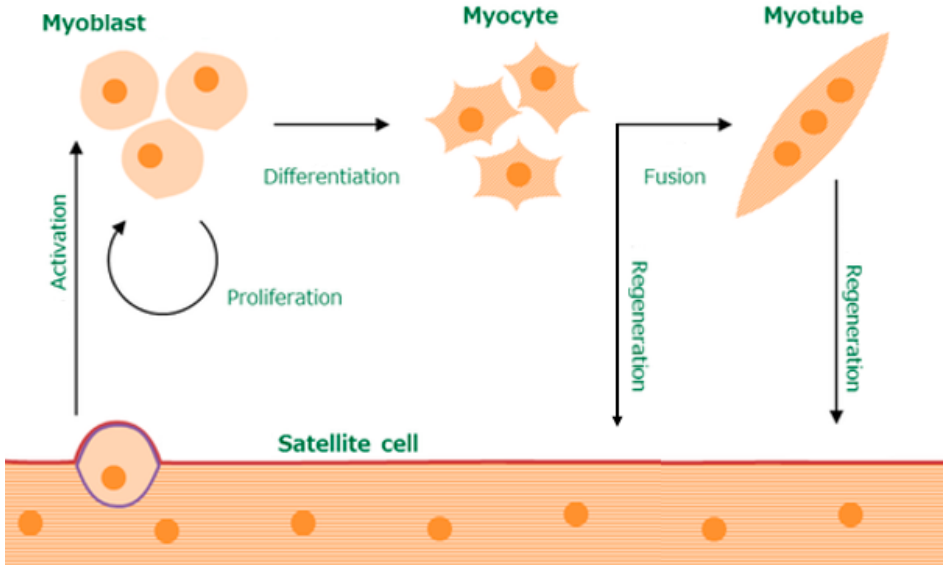

Illustration 1: Schematic of satellite cell muscle repair. SCs reside along the longitudinal axis of adult myofibers. Upon activation they proliferate to repopulate the stem cell pool and differentiate to fuse with new or existing myotubes to repair damaged muscle tissue.

human myopathies and create novel muscle therapies.

Myocyte cytoskeletal networks

The skeletal muscle cytoskeleton is a complex, intricately organized set of proteins essential in virtually all cell functions. The cytoskeleton is comprised of 3 main filaments: microfilaments, microtubules and intermediate filaments.[12] Microfilaments are composed primarily of filamentous actin which form upon polymerization of globular actin monomers. Actin filaments have a plus and minus ends, with more ATP-powered growth occurring at a filament's plus end. Networks of actin filaments allow cells to adapt specialized shapes and are involved in cell division and motility.[13,14] Muscle intermediate filaments are composed of many proteins such as Desmin, Nestin, Lamins, and Cytokeratins.[12] Desmin is the major muscle intermediate filament protein and plays an essential role in maintaining cytoarchitecture.[15,12] Desmin forms a scaffold around the myofibrillar Z-disk and connects the entire contractile apparatus to the subsarcolemmal cytoskeleton, nuclei, and organelles.[15] Microtubules are hollow, straw shaped filaments composed of long strands of protofilaments made of Tubulin.[1,16] Microtubules are involved in cell division, intracellular trafficking, and maintenance of cellular architecture.[16] In non-dividing cells, microtubule networks radiate out from the centrosome to provide basic organization of the cytoplasm and position organelles. All together, these filaments organize into networks which maintain cell integrity and connect organelles.[17] In muscle cells specifically, these filaments also compose highly specialized structures responsible for contraction.

Myocyte contractile apparatus

The basic contractile unit of myocytes, the sarcomere, is comprised of a meticulously organized individual filament system including actin, myosin, nebulin and titin.[12] These contractile proteins chain together in series, to form a rod-like organelle known as a myofibril. The filaments of myofibrils, consist of two types, thick and thin. Thin filaments are primarily composed of actin, coiled with nebulin filaments.[1] Thick filaments consist of myosin, held in place by Titin filaments.[1] The sarcomeric unit is categorized by structural protein filament content. Sarcomeres are bordered by protein dense Z-discs, and its internal regions are classified as A, I, and H bands. The A band contains the entire thick myosin filament including overlapping thin actin filament, I band contains only thin actin filaments, and the H band contains only thick filament.[1] Thin filaments are bound by regulatory proteins Troponin and Tropomyosin, which inhibit the actin activated ATPase of myosin when calcium concentrations are low. When calcium ions bind to troponin, it undergoes a conformational change which removes tropomyosin away from myosin binding sites on actin, and muscle contraction subsequently begins as myosin motor proteins bind to actin. This causes thick and thin filaments to slide against one another, shortening the sarcomeric unit and bringing adjacent Z discs close together. Many regulatory proteins contribute to the alignment and stability of myofibrils. Key regulatory proteins, like Titin, connect the Z disc to the sarcomere, thus stabilizing the position of the thick filament, and Nebulin which regulates the length of thin filaments during development. Alpha-Actinin is another structural protein of Z discs that link actin molecules of thin filaments to Titin molecules. Lastly, within the Z-disc lies the protein

Filamin C, connecting the sarcomere to sarcolemma.[18] This connection is thought to help reinforce the sarcolemma and help transmit tension generated by sarcomeres to tendons. Unique structures like the myotendinous junction (MTJ), the junction between muscle and tendon, constitute a dynamic and functionally integrated unit that transduces mechanical force to the skeletal system for locomotion.[19] The force generated by muscle contraction is transmitted from intracellular contractile muscle proteins to the extracellular connective tissue proteins of the tendon. At the MTJ, where fiber cross-sectional area is the smallest, the sarcomeres must stretch further to balance the forces from larger areas. Thus, the MTJ and its surrounding area, is a common location of injury in skeletal muscle.[20] This specialized region however adapts to excessive stress and tension by maintaining its protein structural integrity. To maintain this integrity under constant stress, many cytoskeletal proteins are upregulated, ready to repair sarcomeres and reinforce their cytoskeletal structures. Moreover, MTJ extracellular matrix proteins like Laminin, Integrin, and Vinculin, enable a strong connection between the muscle actin filaments and the tendon collagen fibers.[21]

Actin cytoskeleton

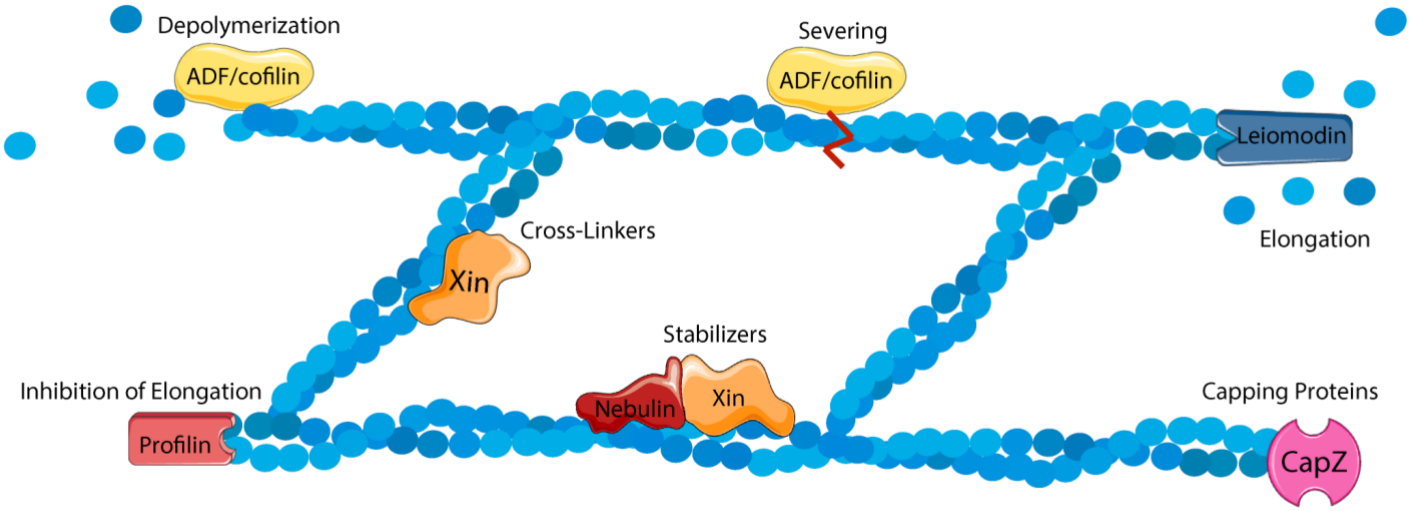

Illustration 2: Dynamic regulators of sarcomeric F-actin. ADF/Co-filin proteins facilitate depolymerization and severing of F-actin. Stabilizers of F-actin include Xin and Nebulin, cross-linking facilitated by Xin and other proteins (not shown). Capping and inhibition of elongation is done by CapZ and Profilin respectively.

Soluble monomeric globules of actin interact to form highly dynamic and tightly regulated filamentous actin (F-actin).[22] There are numerous distinct regulators of actin microfilament function and length including nebulin,[23] tropomodulin[24] and Xin-repeat protein family.[25] Tropomodulin and Profilin inhibit actin polymerization at the distal ends.[26] Leiomodin antagonizes tropomodulin and promotes elongation at distal ends. ADF/cofilin enhances actin filament turnover by severing actin filaments and promoting dissociation of actin monomers.[12] Lastly, F-actin stabilizers such as Nebulin and Xin not only stabilize F-actin but also stabilize other thin filament proteins.[13] The actin cytoskeletal network undergoes extensive remodelling during contractions and serves many functions that are critical for muscle plasticity including the generation of force,[27] determination of cell morphology,[22] and regulating organelle size, structure and localization.[28] In fact, mitochondrial-cytoskeletal interactions have been well-

established in coordinating mitochondrial motility,[29] regulating distribution, anchoring [17] , fission[30] , and respiratory capacity[31]. Actin cytoskeletal networks thus play crucial roles in maintaining cytoarchitectures which determine cell morphology and regulating organelle distribution and function. Alterations to actin network protein regulators that go uncompensated may result in detrimental cellular deficiencies and lead to muscular pathologies.

Cytoskeletal remodelling during myogenesis

The formation of a multinucleated muscle fiber from individual myoblasts requires dramatic cytoskeletal rearrangements. [14] During myogenesis, precursor cells must discard their "generic" cytoskeleton and organize a muscle-specific contractile cytoskeleton. This multistep process includes cytoskeletal rearrangements to facilitate myoblast fusion, myotube migration and elongation, and attachment to form a stable adhesion complex. Myoblasts contain actin filaments distributed throughout the cell, dispersed inftermediate filaments, and radial microtubules.[32] As myoblasts undergo the sub-processes of cellular fusion and motility necessary for differentiation, they largely dependent on actin cytoskeletal networks. Current models of myoblast fusion indicate F-actin remodelling and protrusions are necessary to enhance membrane proximity.[33] Specifically, the coordinated polymerization of multiple actin filaments produce protrusive forces which are important for whole-cell migration. Thus, F-actin protrusions facilitate close proximity of cells necessary for fusion. [27] This highlights the importance of F-actin accessory proteins during differentiation which control F-actin elongation, cross-linking, disassembly, and interaction with other cellular structures. Differentiated myotubes are characterized by strong myofibrillar structures and cytoskeletal

networks. Intermediate filaments are present around Z-lines, microtubules dispersed throughout the cell with no organizing center, and actin filament networks appear throughout the cell but organize either in myofibrils or close to the sarcolemma.[32]

Skeletal muscle calcium regulation

Excitation contraction coupling

To generate and maintain force, muscles require sufficient intracellular calcium stimulus to support excitation-contraction coupling (ECC). ECC links action potentials (AP) generated at the sarcolemma to stimulate muscle contraction.[1] A depolarized sarcolemma sends an AP down T tubules, triggering SR calcium release. Specialized muscle structures known as triads, form the anatomical basis whereby terminal cisternae of the SR are in close association with T-tubules.[1] The tight spatial organization of the triad ensures efficient activation of Ca^{2+} release from SR stores upon membrane depolarization.[34] Specifically, a depolarized T-tubule is sensed by the voltage sensor dihydropyridine receptor (DHPR) which are located at the T-tubule membrane and coupled to SR calcium release channels such as Ryanodine receptor-1 (RyR1).[34] Voltage activated DHPRs then open RyR1 channels to release calcium from the SR. Free cytosolic Ca^{2+} then binds to troponin, causing the troponin to change shape and remove the tropomyosin from myosin binding sites. Myosin heads on thick filaments are then free to bind to thin filaments for muscle contraction.[1] Calcium is then cycled back into SR stores from the cytosol via ATP-powered SERCA pumps.[35] Many calcium-related binding proteins work in concert to transport and maintain calcium release and reuptake during muscle contractions. Calsequestrin (CSQ) sequesters calcium in the SR lumen. Specifically, the primary function of CSQ is to provide high local [Ca^{2+}] at SR-T Tubule junctions and to communicate changes in luminal Ca^{2+}

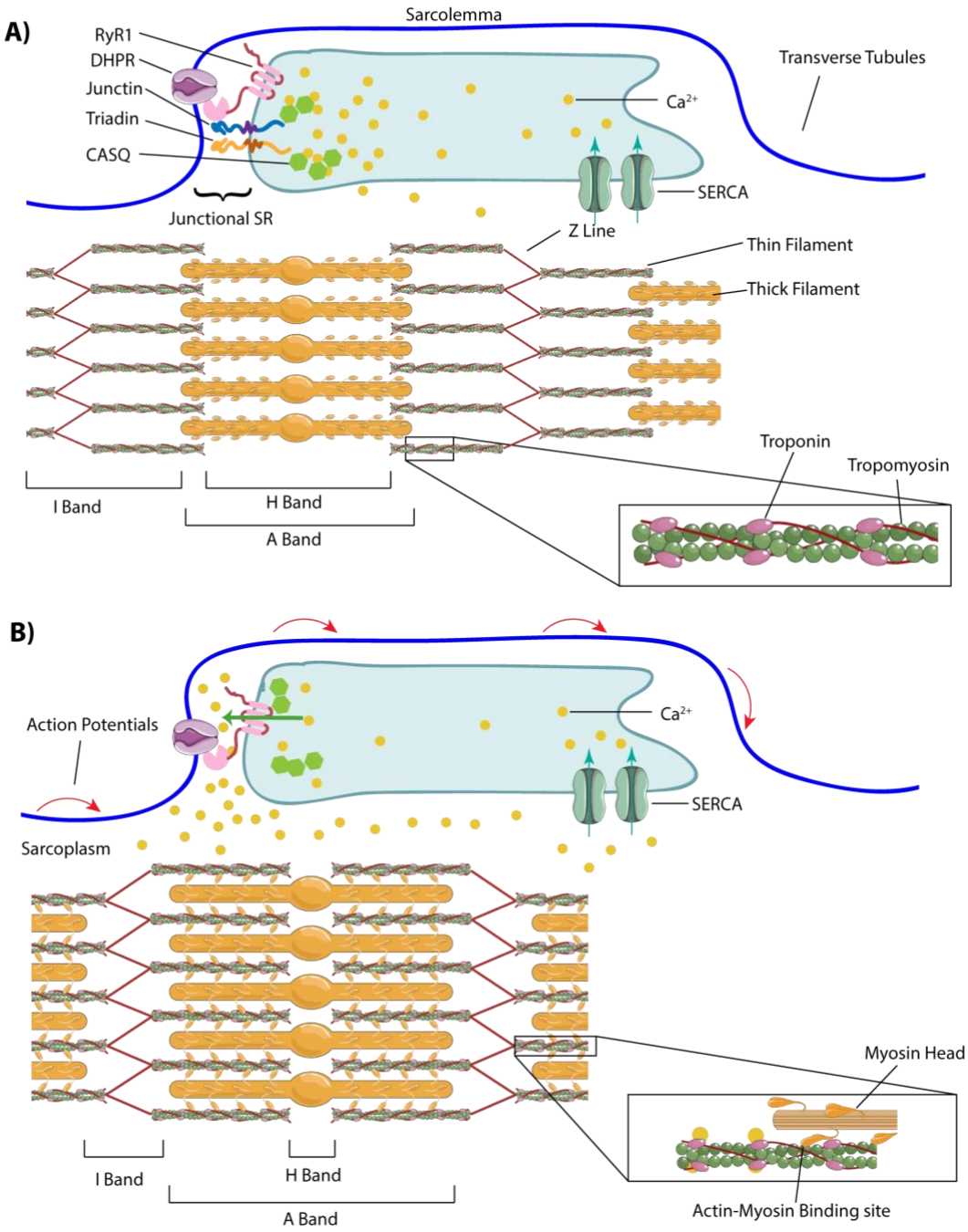

Illustration 3: Illustration of Excitation-Contraction coupling. **A)** Sarcomere relaxation. Sarcomere is composed of thick myosin and thin actin filaments, with actin anchored at Z lines defining the sarcomere border. Sarcomere can be broken up into I band containing only thin filament, H zone containing only thick filament, and A band containing the whole thick filament. Sarcoplasmic Ca^{2+} is low and Troponin and Tropomyosin blocks the binding of myosin heads. SR Ca^{2+}release channels are closed and Ca^{2+} active transport pumps are functional. **B)** Sarcomere contraction. Muscle action potential propagates along the sarcolemma into T-tubules, Ca^{2+}release channels open, Ca^{2+} enters sarcoplasm, binds to troponin, and moves tropomyosin away from myosin binding sites on actin allowing the contraction cycle to begin.

concentration to Ca^{2+} release channels.[36] CSQ interacts directly with junctional SR

transmembrane proteins, Triadin and Junctin, which form a quaternary complex with Ryanodine Receptors (RyR) to inhibit calcium release during relaxation.[36] This inhibition of calcium release, supports the accumulation of high Ca^{2+}levels near the RyR release channel for immediate release timed with action potentials to trigger muscle contraction.

Store operated calcium entry

When SR-Ca^{2+} stores diminish from continuous muscle contractions, the myofiber will replenish Ca^{2+} from the extracellular environment through a process known as Store Operated Calcium Entry (SOCE).[37] Functionally this serves to prolong muscle endurance and support rapid recovery. In short, STIM-1 mediated calcium entry is initiated by SR Ca^{2+} depletion which is detected by SR- membrane bound Stim-1. As Ca^{2} is depleted in the SR, Stim-1 oligomerizes or dimerizes upon dissociation of Ca^{2}. This activation causes Stim-1 oligomers to translocate to the plasma membrane where it binds to and opens membrane-bound store operated calcium channels Orai1 and Transient receptor potential cation channel (TRPC) members. [37,38,] Interestingly, TRPCs are not only mediators of extracellular Ca^{2+} entry in skeletal muscle, but have also been proposed to participate in migration and differentiation of C2C12 myoblasts via calpain activation. [39] On a side note, studies by Mazères et al, demonstrate calpains are calcium sensitive proteases implicated in locomotion of muscle cells. [40] One such substrate of calpains are myristoylated alanine-rich C-kinase substrate (MARKS). MARCKS is an actin-binding protein involved in both myoblast fusion and migration, and is activated by calpain proteolysis.[39,41] Inhibiting calpains in C2C12 myoblasts regulates cell migration negatively, by inhibiting new focal adhesion formation between the cell and the ECM and destabilizing the actin

cytoskeleton. [40] When myocytes do not require SOCE activation, TRPCs are stabilized and kept functionally inactive by a scaffolding family of adaptor proteins Homer.[39] On a molecular level, this inactivation occurs by Homer cross-linking TRPC channels with IP3R and RyR, thus

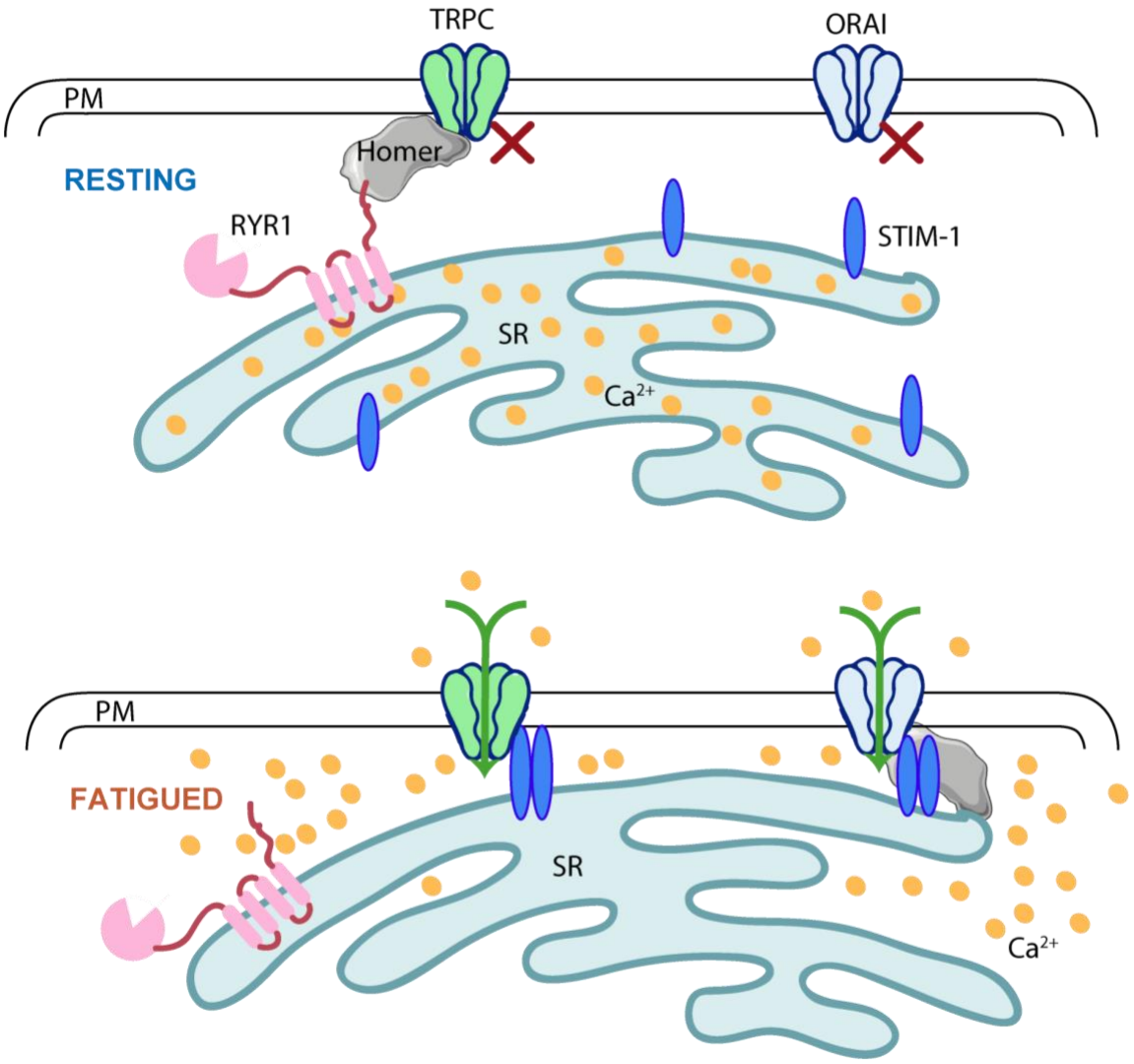

Illustration 4: Store operated calcium entry. A resting myofiber contains ample stores of calcium in the sarcoplasmic reticulum and Stim-1 calcium sensor monomers are bound to the SR membrane. Homer maintains TRPC channels in a closed configuration, complexed with RYR1. Fatiguing contractions deplete SR calcium stores. This depletion is sensed by Stim-1, upon which is dimerizes and translocates to activate ORAI channels on the plasma membrane to facilitate entry of extracellular calcium to the sarcoplasm. ORAI activation is kept open and stabilized by Homer.

modulating the cross talk and Ca^{2+} signaling among these molecules.[42] Upon calcium depletion,

SOCE activation is required and Homer dissociates from TRPC, removing it's inhibitory effect to allow for Stim-1 mediated TRPC activation. [43,42] Additionally, Homer proteins act as a mediator for Stim1's negative regulation of voltage operated Ca^{2+} channels (VGCC) and Stim-1's activation of store operated Orai channels.[44,45] Specifically, upon Ca^{2+} depletion, Homer, STIM1 and Cav1.2, form a complex that inhibits VGCCs. This interference of VGCCs during SOCE likely prevents a further and significant increase in cytosolic Ca^{2+} in response to Ca^{2+} store depletion. In summary, STIM1 negatively regulates Ca^{2+} entry through voltage gated calcium entry but positively regulates SOCE through ORAI1 interaction via a functional Homer.[45]

Xin

Biochemistry of Xin (CMYA-1)

An important F-actin binding cytoskeletal regulator is Xin. It was discovered in 1999 by Wang et al, where differential mRNA display revealed a transcript markedly upregulated during embryonic cardiac looping process of chicken heart.[46] The protein was named Xin, the Chinese character for heart in pronunciation. In humans, its gene is encoded on chromosome 3, and entitled XIRP1 (formerly, CMYA1; cardiomyopathy-associated 1), comprising one large coding exon which gives rise to three different isoforms, A, B, C, due to intraexonic splicing events. Isoform A is the full length product (198kDa) containing 16 amino acid Xin repeats[47]. These repeats define an F-actin-binding motif and therefore identifies Xin-repeat proteins as members of the plethora of actin-binding proteins. Other features of the full length product include a putative DNA-binding domain, amino-terminus proline rich region (PRR) including an EVH1 domain binding consensus motif, which is capable of interacting with EVH1 domains of other proteins like Mena/VASP[25] and nebulin/nebulette during myofibril development.[48] The PRR in

the carboxy terminus contains a Src-homology 3 domain (SH3), with the potential of binding to other signalling molecules via SH3 domain mediated interactions.[46,49] Most strikingly, the carboxy terminus is capable of interacting with Filamin-C, which is important in the assembly and repair of myofibrils and their attachment to the sarcolemma. [25] Isoform B (122kDa) is identical to full length isoform A, however it lacks a C-terminus and hence a filamin-C binding domain. The last is Isoform C which lacks an amino terminus, Xin-repeats, most of the proline-rich regions and beta-catenin binding regions. [50] Xin's characteristic structural motifs allow for an impressive variety of binding partners making it an integral part of a large cytoskeletal protein network. The expression of Xin appears to be restricted to cross-striated muscle and its precursors.[46] During early embryonic development, Xin is detected in both cardiogenic cells of the heart tube and in somites of the mesoderm.[51] In the adult phase, sub-cellular localization studies of the three Xin isoforms in rat cardiomyocytes revealed that all Xin proteins target to myofibrils, while only Xin A and C are incorporated into the intercalated discs (ICD) and only Xin C can colocalize with alpha-actinin at the Z-disc.[25] In differentiating skeletal muscle cells, Xin A and B interact with F-actin and are found in early myofibril formation and remodelling areas along with their interacting partner Nebulin.[48] As myofibrils matured, Xin A/B dissociated from nebulin and its localization restricted to F-actin. Feng et al, investigated the tissue specificity of Xin A and discovered Xin A in myotendinous junctions (MTJ) and blood vessel walls, but not in neuromuscular junctions and nerve fascicles.[52] Interestingly, Xin is enriched at the ICD of the heart and the MTJ, which are both sites of actin filament anchorage to the plasma membrane.[52,19] The MTJ complex resides at the muscle-tendon interface and is required for the transmission of mechanical force and subsequent locomotion.[19] Muscle tears occurring during

muscle usage generally occur at the MTJ and a number of cytoskeletal re-modellers are upregulated including actin-binding proteins like Xin. [53,19]

Xin and skeletal muscle repair

One of the first discoveries of Xin's role in striated skeletal muscle was it directly binds to F-actin and reorganizes microfilaments into cytoskeletal networks by cross-linking.[46] During muscle repair, significant cytoskeletal remodelling occurs as structural proteins are remodelled

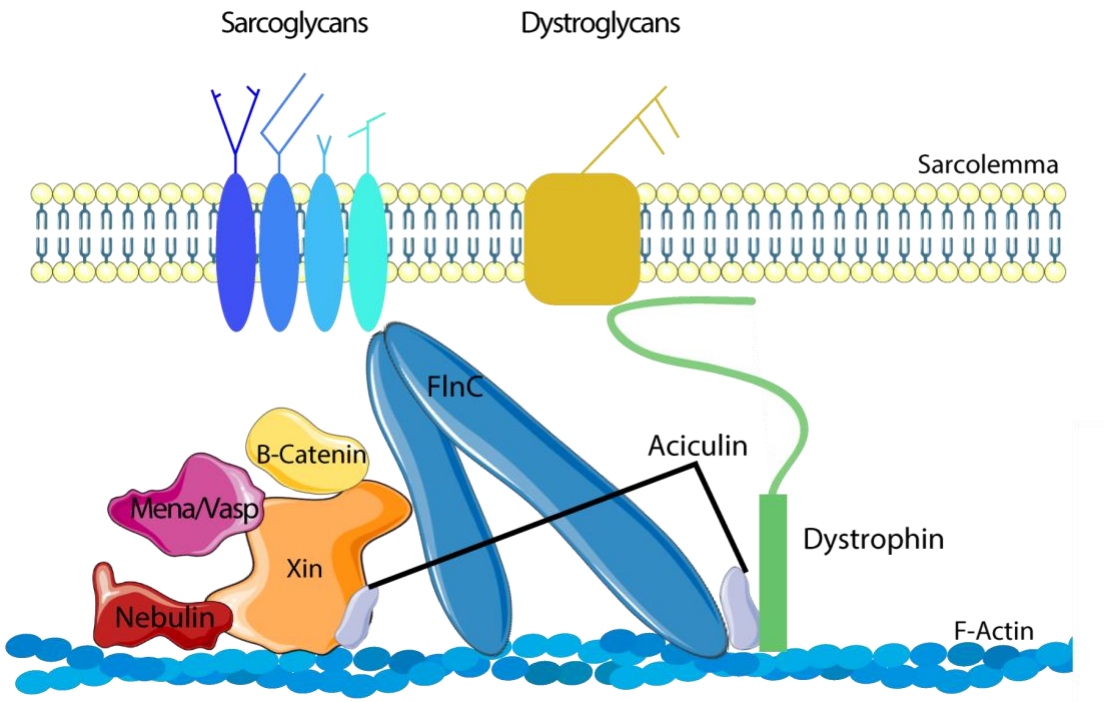

Illustration 5: Xin isoform A and cytoskeletal protein binding partners. Xin isoform A contains actin binding "Xin-repeat" regions that bind to F-actin and organize microfilaments into networks. Xin A is an adaptor protein linking many other proteins together, although not necessarily all at the same time as shown here. It's binding partners include Mena/Vasp and Aciculin which are involved in the regulation of the actin cytoskeleton. Filamin-C binds to Xin and attaches the ends of myofibrils to the sarcolemma. Nebulin binds to Xin and has a similar function of F-actin stabilization. Indirect binding partners include the Dystrophin complex, connecting Xin to a larger cytoskeletal network.

into sarcomeres. The importance of Xin early in regeneration is best demonstrated in its post injury upregulation. Within the first 12 hours of cardiotoxin induced skeletal muscle injury in

mice, levels of Xin mRNA are increased more than 16 fold, indicating the importance of Xin early in regeneration.[50] Furthermore, Xin has also been shown to co-localize with active satellite cells.[54,55] Early studies of *Mus musculus* that depleted all 3 isoforms of Xin (*Xirp1)*, demonstrated a mild cardiac phenotype with altered distribution of intercalated discs, delayed skeletal muscle repair, and impaired satellite cell activation. [47,54] Phenotypic delays in skeletal muscle regeneration are likely a consequence of altered SC functionality. In Xin depleted muscle, SCs exhibited hyperactivation but decreased number of dividing SCs compared to controls.[54] This delay in SC differentiation could be linked in part, due to the importance of cytoskeletal reorganization during differentiation. Therefore, losing an integral F-actin reorganizer such as Xin, resulted in detriments in skeletal muscle regeneration. More recent studies from our lab illustrate Xin -/- muscles are more fatigable and recovered force slower following *in situ* fatiguing contractions compared to wildtype muscles.[56] Moreover, Al-Sajee et al, assessed mitochondrial respiratory kinetics of permeabilized Xin -/- muscle fibers which revealed significant impairments in mitochondrial enzymes complex I and complex II.[57]

Mitochondria and calcium signalling

Ca^{2+} is a critical messenger not only for muscle contraction, but also for promoting mitochondrial ATP production. An increase of free calcium in muscles is required to stimulate the electron transport chain of mitochondria, and thus ATP production. [58] It does so by upregulating the activity of citric acid cycle dehydrogenases to increase the production of reducing equivalents for the electron transport chain. Therefore, mitochondrial Ca^{2+} uptake acts as a local Ca^{2+} buffer and an important modulator of muscle contractions. A study by Rudolf et

al, clearly demonstrates significant mitochondrial Ca^{2+} uptake during single twitches and tetanic contractions.[59] The group demonstrated mitochondria will rapidly take up Ca^{2+} during skeletal muscle contraction and rapidly release it during muscle relaxation. Calcium uptake into mitochondria during contraction may serve to adjust ATP production to match the muscle's physiological demand. Moreover, contractile relaxation is accelerated in mitochondria-rich muscle fibers.[60] To match this high energy demand, calcium is transported into the mitochondria via the mitochondrial Ca^{2+} uniporter (MCU). However, due to the poor affinity of the MCU to Ca^{2+}, the kinetics remain controversial. Recent studies report that although individual mitochondrial Ca^{2+} uptake is limited, mitochondria coalescing together in close vicinity to the SR is sufficient to overcome the MCU's low sensitivity.[61] In addition, it is worth noting mitochondria are dynamic organelles which undergo constant changes in localization, mass, morphology and composition depending on cellular needs.[62] In order to facilitate these dynamics, studies show functional and physical communication between mitochondria and other organelles in muscle, such as the sarcoplasmic reticulum (SR). SR-Mitochondria coupling bi-directionally transfers Ca^{2+} between organelles and is a critical regulator of cell metabolism.[61,63]

Mitochondria – SR Contacts

Mitochondrial associated membrane (MAM) tethers structurally associate SR-Mitochondria organelles in close-contact and function to couple multiple physiological processes such as calcium signalling, lipid exchange, bioenergetics and apoptosis. One such family of MAM tethers are the dynamin-like GTPases, Mitofusin 1 (Mfn1) and Mitofusin 2 (Mfn2). In addition to being

required for mitochondrial fusion, they also bridge the mitochondria onto the ER allowing for efficient Ca^{2+} transfer. [64,65] Another important MAM tether is the voltage dependent anion channel (VDAC) of the outer mitochondrial membrane (OMM). VDAC is thought to be the primary means by which the metabolites diffuse in and out of the mitochondria. In addition to MCUs, Ca^{2+} import across the OMM is transported through VDAC. This calcium transfer is accelerated when VDAC physically interacts with the endoplasmic reticulum (ER) -release channel inositol 1,4,5 triphosphate receptor (IP3R) through the molecular chaperone glucose-regulated protein 75(Grp75). Thus, forming a tripartite complex (IP3R-grp75-VDAC) and tethering the ER and mitochondria in close proximity.[66] This complex will form a microdomain of high [Ca^{2+}] which facilitates mitochondrial calcium uptake through VDAC and near the MCU.[67] MAM subdomains not only allow Ca^{2+}communication but also the interchange of complex lipids. The majority of lipids are synthesized in the ER and transported to the mitochondria to maintain the defined lipid composition of mitochondrial membranes.[68] In contrast, mitochondria contribute significantly to the synthesis of membrane lipids in cells.[69] Consequently, extensive bidirectional lipid transfer occurs between the ER and the mitochondrial outer membrane, facilitated by transfer proteins enriched at MAM sites [68] One such protein regulator of mitochondria-ER cholesterol transfer is Caveolin-1 (CAV1).[70] CAV1 deficient mice have reduced MAM physical extension and aberrant cholesterol accumulation at ER subdomains[70] Comparative proteomic analysis between CAV1 -/- and WT mice revealed Cav-1 contributes to the recruitment and regulation of intracellular steroid and lipoprotein metabolism processes accrued at MAM sites. Together, these studies portray MAMs as an

intracellular signalling hub which coordinates the metabolic status of the cell with other cellular processes.

Xin and mitochondria regulation

Electron micrographs of mouse Xin -/- muscle reveal mitochondria increased in population, were swollen, mis-localized and displayed impaired respiration rates. [71] WT mitochondria are primarily found in a triad adjacent location running parallel to Z-lines. However, mitochondria in Xin-/- skeletal muscle displayed extensive swelling and mislocalization throughout the muscle tissue. Moreover, Xin depletion in muscle tissue significantly blunts mitochondrial respiration rates in ETC complex I and II. Interestingly, while no differences were initially detected in either complex I or complex II, correcting to mitochondrial content indicated significant impairments in Xin-/- muscle at both sites, implying that individual mitochondria may be dysfunctional and that an increase in mitochondrial content appears to compensate for these deficiencies at the whole tissue level.[71] The ability of mitochondria to consume oxygen in response to energy demands serves as a reliable hallmark of its functional state, reflecting cell viability. Thus, Xin depletion resulted in abnormal mitochondria structure, function and localization. Despite current literature lacking physical or functional link between Xin and mitochondria, immunoelectron microscopy analysis of Xin from our lab illustrated its localization as focal aggregates in peri-mitochondrial and mitochondrial spaces within human muscles.[71] Considering Xin localized near mitochondria and its depletion exhibited phenotypic changes similar to other MAM knockout studies, it's been speculated Xin is functioning as a MAM tethering protein. For instance, disorganized triad structures and aberrant mitochondria have

previously been shown to be a result of disrupted autophagosome formation whose precursors localize to mitochondrial associated ER membrane (MAM) sites.[72] Autophagosome formation is necessary to remove dysfunctional mitochondria and inhibiting its formation can result in the accumulation of damaged mitochondria. These phenotypes are shared between Xin KO and inhibition of autophagosome genesis at MAM sites. These similarities therefore provide functional evidence that support a Xin MAM tether theory which needs further investigation.

Xin and calcium regulation

Whole body knockout of Xin in mice leads to a mild myopathic condition characterized by increased muscle fatigability, impaired regeneration and satellite cell dysfunction.[56] Moreover, characterizing the function of these muscles through *in situ* muscle stimulation protocols results in increased fatigability and decreased force recovery following fatiguing contractions compared to controls. Al-Sajee et al, sought to understand the molecular basis of this increased fatigability. Live-cell measuring of free calcium during muscle contractions revealed Xin-/- muscle fibers had impairments in Ca^{2+} release during tetanic contractions and in response to prolonged contractions.[57] This dysregulation in calcium handling was consistent with their previous observations of the inability of Xin-/- muscles to maintain force throughout a tetanic contraction. Moreover, decreased force production and calcium release are analogous to phenotypes of Orai1 knockout muscles. [37] Therefore, since Orai1 is an integral macromolecular component necessary for SOCE, they hypothesized Xin associates with the SOCE complex by directly binding to Homer and Stim-1. This association likely maintains the opening and activation of SOCE complex through stabilization.

Purpose & Hypothesis

Our current scientific understanding of the role and binding partners of Xin within striated muscles is inadequate. Our experiments using a reduction in Xin expression have led to a diverse set of possible functions, such as regulation of intracellular Ca^{2+} and mitochondria stability and localization. To carry out these functions, numerous potential protein binding partners like Calsequestrin, Homer, Stim1, Desmin and other MAM tethering proteins have been proposed. However, it is unclear as to which observed phenotypes are the result of a true direct effect or a compensatory mechanism that cells have adapted to. Thus, the purpose of my thesis was to use an overexpression model of Xin to aid in discovering the function of Xin within skeletal muscle and identify new Xin binding partners within this tissue. We hypothesized that Xin overexpression will impair differentiation and impact myoblast and/or myotube fitness, induce mitochondrial damage, and compromise calcium homeostasis. These various functional impacts are hypothesized to be facilitated by stabilizing other protein complexes such as SOCE and MAM tethers.

Methodology

C2C12 Cell Culture

Proliferating C2C12 cells (ATCC Virginia USA, CRL-1772) were cultured on polystyrene dishes (Fisher Scientific Mississauga, 150350) in growth media containing high-glucose (4g/L) Dulbecco's Modified Eagle Medium (DMEM) supplemented with sodium pyruvate and L-glutamine, 10% fetal bovine serum (FBS) which did not contain penicillin/streptomycin . Cells were incubated at 37°C with 5% CO_2 and kept at 25-80% confluence until passage number ~20. To induce differentiation cells were grown until 95% confluence in time for the switch to differentiation media (high-glucose DMEM with 2% horse serum). Media was changed every two days and live cell images were taken thereafter. Plates were imaged at semi-sterile room conditions. All imaging and analysis were conducted using a Nikon ECLIPISE Ti microscope and Nikon NIS-Elements ND2 software (Melville, NY, USA).

Primary myoblast isolation and culture

Murine hind limb muscles including the tibialis anterior, soleus, and gastrocnemius were dissected in a semi-sterile environment after cervical dislocation. Immediately after dissection, muscles were transferred to 60 mm polystyrene dishes containing Dispase [1.2 U/mL] (Sigma Aldrich Oakville, D4818) and collagenase IV [1.5 U/mL] (Thermo Fischer, 17104019). Tissues were mechanically separated then incubated at 37°C and 5% CO2 for 45 mins. After, the muscle slurry was washed in 15 mL of 1X phosphate buffered saline (PBS) (free of Ca^{2+} and Mg^{2+}) containing 100 mM D-glucose. The slurry was then centrifuged (400 *g*, 4 mins) and resuspended in 10 mL of 0.05% Trypsin-EDTA then incubated 37 °C and 5 % CO2 for 1.5 h.

Proliferation media (10 mL; 20% FBS, 0.5% Chicken Embryo Extract, 4 g/mL glucose) was added to deactivate trypsin and the slurry was filtered through a 100 µm nylon mesh before being centrifugated at 400 g, 4 °C for 4 mins. Following centrifugation, the pellet was suspended in 10mL of proliferation media and pre-plated for 1-2 hrs on an uncoated 100 mm polystyrene dish (Becton Dickinson Labware, Franklin Lakes, NJ. USA). Finally, media containing non-adhered myoblasts were seeded on 1% GelTrex (Thermo Fischer, A1413201) coated plates. 5-7 mLs of diluted GelTrex was added to 100mm plates and stored at 4 °C. GelTrex was activated by heating plates at 37 °C , 5 % CO_2 for 1 hour and aspirating leftover media. Cells were incubated for 5 days in proliferation media in incubator and media was changed every 2 days. Myoblasts were then induced to differentiate by switching to differentiation media (high-glucose DMEM with 2% horse serum). Mature myotubes were then used for downstream applications like adenoviral infection and subsequent semi quantitative-PCR analysis.

Adenovirus Infection

To increase endogenous Xin expression (mouse), C2C12 cells were incubated with a custom recombinant designed XIRP-1 (Applied Biological Materials, Richmond BC, C070-42417) C-terminally tagged with human influenza hemagglutinin (HA). The adenoviral system is driven by a strong cytomegalovirus promoter, replication incompetent due to E1/E3 deletions and human adenovirus type 5. Cells were washed once with warm sterile PBS and incubated with trypsin for 5-10 mins at 37°C, 5% CO2. Cells were counted using a hematocytometer (Hausser Scientific Pennsylvania, 3800) each plate was seeded with 200,000 cells and given 2 hours to adhere. Following adherence, cells were infected for 6 hours. Viability of cells was accounted for by 0.4% Trypan Blue staining (Thermofisher Scientific, 15250061). For the duration of the

infection, cells were kept in low volume of growth media (300 µL) to promote virus incorporation. Control cells were infected with empty vector adenovirus (Vector Biolabs Pennsylvania,1240). After infection, cells were returned to normal confluence in growth media for 24 hours to allow for sufficient protein production. Protein overexpression was verified by western blot before continuing downstream applications.

Live-cell cytochemical staining

MitoTracker Red CMXRos (Thermo Fischer, M7512) and DAPI (Thermofisher, D1306) were diluted in sterile growth media at final concentrations of 50nM and 10 µg/mL respectively. Cells were seeded in Falcon® 4-well culture glass slide with polystyrene vessel. At ~75% confluence, cells were incubated in the staining solution under normal culture conditions for 30mins, washed briefly in 1X PBS, and then visualized by fluorescence microscopy (ECLIPSE Ti, Nikon). Cells were imaged for 30mins at standard room temperature and semi-sterile conditions. Multichannel exposure times were set to negative control slides. For visualization of Xin and MitoTracker, cells were fixed after MitoTracker staining and proceeded to immunocytochemical staining for anti-HA. We excluded 0.3% Triton X-100 permeabilization as this causes MitoTracker to leak out of the cell plasma membrane.

Western Blot

C2C12 cells for western blot were washed in ice-cold 1X PBS twice for 5 mins and then scrapped in ice cold SBJ lysis buffer containing 50 mM HEPES, 150 mM NaCl, 100 mM NaF, 10 mM Na pyrophosphate dibasic, 5 mM EDTA Na_2, 250 mM Sucrose, 1 mM DTT, protease inhibitor

cocktail (Thermo Fisher Scientific), 1 mM sodium orthovanadate, 1% Triton X-100. Samples were sonicated (Qsonica Connecticut, XL2000) for 10 sec ON/OFF cycles at 10% power for 2 mins, rotated at 4°C for 1 hour and then centrifuged at 12,000 rpm for 10 mins at 4 °C. Supernatants were collected and then stored at -80 °C until analysis. Protein concentrations were determined using a Pierce BCA assay (Thermo Scientific, 23223) and to ensure protein quantity was loaded equally. Western blot intensities were normalized using 1X Amido Black staining solution (Sigma, A8181-1EA). Proteins were separated by 10% SDS-PAGE (100 V for 75 mins) and then transferred to nitrocellulose membrane (90 V for 90 mins at 4 °C). Membranes were incubated in blocking buffer (5% BSA in 1X TBS-T or 5% Skim Milk in 1X TBS-T) for 1 hour at room temperature and incubated overnight at 4°C using commercially available antibodies validated by manufacturers for western blotting: mouse anti-HA tag- 1:1000 (Cell Signalling Technologies CST Massachusetts, 6E2), rat polyclonal anti-Homer 1b + 1c 1:1000 (Abcam Massachusetts, ab18550), mouse anti-Triadin 1:500 (Thermo Fischer, MA3-927), rabbit anti-Junctin 1:500 (Sigma Aldrich, AV51356), rabbit anti-Calsequestrin-1 1:1000 (Abcam, ab191564)**,** mouse 1:500 anti-Myogenin 1:1000 (ThermoScientific, MA1-41042), rabbit 1:1000 anti-Vinculin (CST, 4650), mouse 1:2000 anti-GAPDH (Applied Biosystems, AM4300), rabbit anti-Histone H3 (CST, 9715), mouse 1:250 anti-Total OXPHOS rodent antibody (Abcam, ab110413), 1:1000 mouse anti-Caveolin- 1 (BD Biosciences Mississauga, 610406), rabbit 1:1000 anti-Stim-1 (Sigma Aldrich, S6196) rabbit 1:1000 anti-Orai-1 (Thermo Scientific, PA5-20402) mouse 1:1000 anti-Filamin-C (Novus Biologics Oakville, FLM01), mouse anti- 1:1000 Mitofusin 1+2 (Abcam, ab57603), mouse 1:1000 anti-Mitofusin 2 (Abcam, ab56889), rabbit 1:1000 anti-Parkin (Abcam, ab15954), rabbit 1:1000 anti-VDAC 1 (CST, D73D12). Membranes were then washed in tris-

buffered saline, 0.1% (vol./vol.) Tween 20 (TBS-T) three times rocking for 10 mins each and incubated for 2 hours at room temperature in horseradish peroxidase conjugated secondary antibody. The following secondary antibodies were used: HRP-linked anti-rabbit IgG, (CST,7074) HRP-linked anti-mouse, (CST,7076) and HRP-linked anti-rat (CST, 7077). Membranes were washed in TBS-T three times for 10 mins each and immunoreactive proteins were detected were visualized using chemiluminescent reagent (BioRad Mississauga, 1705061) and detected using a gel image system (Montreal BioTech, Fusion Fx7). Western blot band densitometry was quantified using ImageJ (v2.0.0-rc-69/1.52p).

Semi-quantitative RT-PCR and Analysis

Cellular RNA extraction and purification was completed following the manufacturer's protocol for PureLink ^{tm} RNA MiniKit (Invitrogen, 12183018A). RNA concentration and purity was assessed using a NanoPhotometer (MBI). Total mRNA was reverse transcribed to complementary DNA (cDNA) using Superscript III reverse transcriptase (Invitrogen, 18080093) random hexamers (Invitrogen, N8080127). First strand cDNA synthesis was performed according to manufacturer's protocol. Amplicons from cDNA template was amplified by polymerase chain reaction (conditions: *1)* 94° for 2 mins, *2)* 94°, 1min *3)* 54.5°, 45s *4)* 72°, 1min; steps 2-4 repeated 35 times, *5)* 72° 5 mins) PCR primer sequences used are as follows: Xin (Fwd 5'-CAGGTAGTTGGAGGTGATGTT -3' , Rvs 5'- TCTGCTGGGTTCAGAGATTG-3') 18S (Fwd 5'-CCGCAGCTAGGAATAATGGAATA-3' , Rvs 5'- CCTCTAGCGGCGCAATACGAAT-3') GAPDH (Fwd 5' GTGGCAAAGTGGAGATTGTTGCC-3' , Rvs 5'-GATGATGACCCGTTTGGCTCC-3'). Amplicons were then diluted into 6X loading dye (iNtRON, 21161) and run on diluted EtBr 2% Agarose gels for

1.15Hrs at 130V. Band fluorescence was visualized using gel imaging system (Fusion Fx7, MBI) and band densitometry analyzed with ImageJ (v2.0.0-rc-69/1.52p).

Migration Scrape Assay

Following adenoviral infection, 95% confluent 60mm plates were laterally dragged with a razor blade to remove C2C12 cells from one side of the scratch line. Plates were rinsed thoroughly to remove detached C2C12 cells. At 0, 6 and 24 hour time points 8 images were obtained along the land-marked scratch line using an inverted microscope (Nikon Eclipse TE2000U). C2C12 mean distance migrated was calculated by averaging results from all 8 image measurements.

Immunocytochemical staining

C2C12 myoblasts were seeded onto culture slides (BD Biosciences, 354104) and then infected with either ADV-HA-Xin or ADV-Null and incubated for 24 Hrs to allow for ample protein production. Wells were washed 3 times for 5 mins in warm 1XPBS and later fixed in 4% paraformaldehyde for 7 mins at room temperature. Wells were washed in cold 1X PBS (5 mins X3) and blocked for 1 hour at room temperature. Blocking reagent contained 5% normal goat serum (Vector, S-1000), 0.3% Triton X-100 (BioRad, 1610407) diluted in 1X PBS. Primary antibody mouse anti-HA tag- 1:100 (CST, 6E2) diluted in antibody dilution buffer was added in enough volume to cover slides and incubated overnight at 4°C. For visualization of mitochondria and Xin, a cocktail of mouse 1:100 anti-COXIV (Abcam, ab33985) was mixed with rabbit 1:100 anti-HA tag (CST, C29F4). Antibody dilution buffer contains 1% dissolved bovine serum albumin (Thermo Fischer, 12483020) and 0.3% Triton X-100. Wells were washed in cold

1XPBS (5 mins X3) and Alexa Fluor™ 488 goat anti-mouse IgG1 (Life Technologies, MG120) 1:2000 for 2 hours at room temperature in dark. Wells were washed in cold 1XPBS (5 mins X3). For visualization of cellular F-actin a working solution of Alexa Fluor™ 594 Phalloidin (Invitrogen, A12381) was added and incubated for 20mins at room temperature in the dark. Wells were washed in cold 1XPBS (5 mins X2) and then counterstained in DAPI for 5mins room temperature. Slides were briefly washed again in 1X PBS and then mounted in fluorescence mounting medium (Agilent Technologies Mississauga, S3023). Slides were dried overnight in the dark and then visualized using fluorescence microscopy (ECLIPSE Ti, Nikon). Multichannel images were taken using DAPI (Ex 360, Em 460), FITC (Ex 498, Em 520) TRITC (Ex 552, Em 578) filter cubes.

Coimmunoprecipitation

Co-immunoprecipitation to elute HA-tagged fusion proteins and their binding partners was done using immobilized anti-HA affinity resin from Pierce™ Anti-HA Agarose kit (Thermo Fisher, 26181). Cells were infected with either ADV-HA-Xin or ADV-Null and incubated for 24 Hrs to allow for ample protein production. Cells were lysed in non-denaturing SBJ lysis buffer (cocktail above) and sonicated for 10 sec ON/OFF cycles at 10% power for 2 mins, then centrifuged at 12,000 rpm for 10 mins at 4°C. Supernatants were collected and protein concentration was quantified using BCA assay (Thermo Scientific, 23223). 600 μg of protein was loaded with antibody linked resin and the co-immunoprecipitation procedure was followed according to manufacturer's guidelines. We followed SDS elution protocol for characterizing protein fractions via western blot.

For VDAC coimmunoprecipitation assays, 200 μL of cell lysate [1mg/mL] was first pre-cleared by adding 20 μL of Protein G PLUS/Protein A-Agarose (Calbiochem San Diego, IP05) for 1 hour with rotation at 4 °C. To remove beads and nonspecific proteins, we centrifuged at 14,000 g for 10mins 4 °C and collected supernatant. Primary rabbit 1:100 anti-VDAC 1 was added and incubated O/N rotation at 4 °C. The next day we added 20 μL of Protein G PLUS/Protein A-Agarose and incubated 4 hours with rotation at 4 °C. We then centrifuged for 30 s 14,000 g to pellet beads and supernatant flow-through and wash fractions. To elute, we first resuspended pellet with 20 μL of 3X non-reducing SDS buffer by vortexing briefly. To capture eluent, we then heated the sample to 95 °C for 5 mins then microcentrifuged for 1 min at 14,000 g. Supernatant was collected, diluted to 1X elution concentration and prepared for western blot analysis.

Mitochondrial Isolation

C2C12 cells myoblasts were terminally differentiated to mature myotubes over the course of 7 days in a 100 mm 1% GelTrex coated dish. On day 5, cells were infected with 60-80 μL of ADV-Ha-Xin. After 48 hours of incubation, cells were trypsinized then washed with ice cold 1X PBS (with of 100 mM Ca^{2+} and Mg^{2+}). Total protein yield was then calculated via BCA assay. Mitochondria were then isolated using a mitochondria isolation kit for cultured cells (Abcam, ab110170) following manufacturers protocol. Crude mitochondrial fractions were then assessed for purity via western blot by measuring cytosolic and nuclear markers, and then used for downstream applications such as co-immunoprecipitation.

Statistical Analysis

All statistical analysis was conducted using GraphPad Prism 7.0. All results are expressed as mean ± standard deviation. An unpaired students *t*-test was performed for all statistical analysis with the exception of measuring myotube and myoblast morphology which a 2-way ANOVA and Bonferroni's *post hoc* analysis was done. Significance was established as $P<0.05$.

Results

Validating recombinant *XIRP1* transcriptome and Xin protein overexpression

To evaluate the efficacy of adenoviral mediated Xin overexpression and knockdown systems in C2C12 myoblasts and primary myoblasts we utilized western blot and semiquantitative PCR techniques. We confirmed HA-Xin protein expression was dose dependent *in vivo* by blotting for the unique HA tag from cellular lysates (*Fig.1)*. Moreover, HA tagged Xin appears at the expected molecular weight of 150kDa. To confirm Xin overexpression at the transcriptome *(Fig.2)*, primary myoblasts and C2C12 myoblast RNA was extracted, purified then reverse transcribed to cDNA templates. Expression of *XIRP1* and *GAPDH, 18S* controls were assessed using semiquantitative PCR (sqPCR). Normalized *XIRP1* gene expression displayed a doubling of *XIRP1* content in both isolated primary myoblasts *(Fig. 2A)* and C2C12 myoblasts *(Fig.2B).* Adenoviral mediated XIRP1 knockdown was effective at approximately halving gene expression and infecting myoblasts with both overexpression and knockdown systems rescued normal XIRP1 gene expression relative to the adenoviral empty vector control *(Fig. 2B).*

Xin overexpression had no discernable effect on myoblast morphological features or survival

Myoblast features were assessed 24 hours post adenoviral infection with Xin OE vector or empty vector control using light microscopy. No morphological differences in mean area or length were noted between Xin overexpression cells and control *(Fig.3)*. Slight decrease in cell survival was noted however at higher Xin MOI titrations (87%) but does not significantly impact cell confluence. Otherwise, there was no difference in cell survival of Xin overexpressing myoblasts compared to control *(Fig.3B)*.

Recombinant Xin overexpression attenuated normal cell differentiation

To examine whether full length Xin overexpression in myoblasts affected differentiation, we first measured myotube terminal lengths at day 7 of differentiation. This revealed myoblasts overexpressing Xin induced to differentiate had a decreased average myotube diameter dependent on MOI *(Fig.4A)*. In comparison to control, terminal length decreased by 29% (P<.001) for MOI 100 , 25% (P<0.05) for MOI 300, 42% (P<.0001) for MOI 500, and 22% (no statistical significance) for MOI 700. Next, we investigated at what point in the differentiation time course does Xin OE reduce myotube lengths. We measured individual myotube lengths *(Fig.4B)* and widths *(Fig.4C)* at days 3, 5 and 7 of differentiation. The lengths of myotubes infected with the adenoviral construct overexpressing HA-Xin were decreased at day 5 compared to control myotubes (20%; P<.001) and further decreased at day 7 (60%; P<.0001). No effect was observed on the width of myotubes exposed to an increase in Xin in comparison to control myotubes. Xin overexpression (MOI 500) diminished nuclear accretion in myotubes as noted by decreased proportion of highly multi-nucleated myotubes (>10 nuclei) and significantly increased proportion of less nucleated myotubes (<4 nuclei) *(Fig.5A).* A further decline in myotube nuclear

accretion was observed as Xin expression increases with higher MOI titres *(Fig.5B)*. No differences in western blot intensities for terminal differentiation markers, myosin heavy chain and Myogenin, were observed compared to control when normalized to vinculin.

Xin overexpression had no effect on average mitochondrial membrane potential but increased mitochondrial enzyme content

No change in average MitoTracker intensity signal per cell was observed between Xin overexpression and control in C2C12 myoblasts independent of MOI *(Fig.6B)*. MitoTracker accumulation is dependent on differences in mitochondrial membrane potential. Enriching mitochondria from cell lysate reveals increased OXPHOS western blot intensity (~ 2.94 fold increase) of Xin OE myoblasts compared to control in technical triplicates *(Fig.6D)*.

Xin overexpression decreased myoblast migration

As myoblast migration is an important component to their ability for fusion[7] we investigated migratory capacity via scrape assay to determine if Xin OE impacted myoblast migration. At 24 hours post-adenoviral infection and ~90% cell confluency, cells were scraped from one side of a starting line and cell distance from the starting line was recorded at 6 hours, and 24 hours later. We observed that Xin OE cells were unable to migrate as far as control treated cells at 6 hours (~45% less) and 24 hours (~32% less) *(Fig. 7)*. Measuring area under curve for average distance of cells revealed a statistically significant decrease ($P<0.05$) in cell migration of Xin overexpressing myoblasts compared to control *(Fig. 7B)*.

Xin overexpression does not change F-actin distribution

Xin overexpression resulted in no changes to F-actin distribution independent of MOI *(Fig. 8B)*. F-actin was stained using an Alexa conjugated phalloidin and its distribution within the cell was quantitatively assessed using a freely available ImageJ macro by Zonderland et al.[73] Staining intensities in subcellular compartments (nuclear, cytosol) are measured automatically along a drawn line over the cell. The average phalloidin intensities in subcellular compartments corresponded to F-actin quantities, and the difference between them to F-actin distribution. Moreover, there is remarkable visual overlap in localization and intensity between Xin and F-actin *(Fig. 8A)*. Therefore, Xin did not visually deviate from its expected localization and is likely binding to F-actin.

Xin co-localizes to mitochondrial markers

MitoTracker staining in combination with immunocytochemical staining for Xin in C2C12 cells revealed a high degree of signal overlap and intensities *(Fig. 9A)*. We then quantified this overlap using colocalization analysis tools Mander's overlap coefficient (MOC) and Pearson's correlation coefficient (PCC) between MitoTracker and Xin per cell. PCC quantifies the degree to which variability in pixel intensities can be explained with a linear relationship, and is sensitive to both signal co-occurrence (the spatial overlap the probes) and signal proportionality (probes co-distribute in proportion to one another).[74] Unlike Pearson's, MOC is almost independent of signal proportionality, and instead it is primarily sensitive to signal co-occurrence. We used both analysis tools to assess both overlap distribution and proportionality of the two probes with the aim of confidently testing whether Xin occupies mitochondrial structures. We

observed a high degree of overlap in mean MOC (~95%) between MitoTracker and Xin *(Fig. 9B)* and a moderate PCC ~ 0.45 (*Fig. 9C)*. These observations were independent of MOI. The high MOC informs us there is a large degree of co-occurrence between Xin and MitoTracker. Meanwhile, the PCC reported a moderate positive linear correlation between the superimposition and intensity of the pixels. To provide further evidence of mitochondria and Xin overlap, we repeated this experiment using another mitochondrial marker (COXIV) to visualize mitochondria subcellular localization (*Fig. 10A)*. The antibody approach to visualize mitochondria was preferable, as we can observe mitochondria in higher resolution and visualize features such as individual punctate and small networks. There is a strong mean Mander's overlap percentage ~71% *(Fig. 10.B)* and Pearson's correlation coefficient ~0.68 *(Fig. 10.C)* between intracellular Xin and COXIV signal.

Xin is present in mitochondrial fractionations

Enrichment of mitochondria from whole cell lysates revealed Xin's presence in mitochondrial fractions Assessing mitochondrial isolation efficacy and purity by western blotting for mitochondrial, cytosolic and nuclear markers revealed the mitochondrial isolation was imperfect. Although there is a strong increase in intensity for mitochondrial enzymes in crude mitochondrial fractions there is also cytosolic and nuclear contaminations present. To compensate for non-mitochondrial entities present in mitochondrial fractions which could artificially inflate Xin's quantity, we normalized Xin to Gapdh and total histone sum intensity *(Fig. 11B)*. We observe Xin is indeed present in mitochondrial fractions and there is 42% less Xin in mitochondrial fractions compared to lysate controls *(Fig. 11).*

Bioinformatic analysis identifies novel protein-protein interactions

Candidate protein interactors were investigated using STRING and GeneMANIA Cytoscape in the organism *Mus muscularis*. *XIRP1* queries were programmed using a "guilt by association approach" which states that genes with related function tend to be protein interaction partners or share features such as expression patterns. Novel interactors were given scores for genetic co-expression, experiment, and text score. These scores were then compiled into a total output score which candidates were ranked *(Fig. 12B)*. We suspect Xin could be playing a role in balancing calcium homeostasis and/or mitochondrial autophagy based on observed phenotypes from full Xin knockout studies in mice such as susceptibility to muscle fatigue and abnormal mitochondrial morphology. Candidate proteins which could provide a functional basis for these observations include calcium ion homeostasis proteins: Calsequestrin, Homer, Triadin and Junctin *(Fig. 12A)* and mitochondrial proteins such as Mitofusin 1/2 *(Fig. 13A)* and VDAC1 *(Fig. 13B)*.

Xin interacts with calcium related proteins

To interrogate the molecular weight profiles of proteins which co-immunoprecipitated with Xin, we analyzed Co-IP fractions via Coomassie staining of an SDS-PAGE gel *(Fig. 14)*. After identifying the molecular weights of bands present in the elution fraction, we then sought out to pair those molecular weights with both predicted and known protein interactors. Now that our bioinformatic predictions were grounded with molecular evidence, we next sought to verify these interactions via western blot. Blotting for calcium related interactors *(Fig. 15)* we observed

bands present at the expected molecular weight in elution fractions for proteins Triadin, Caveolin, Stim-1, Homer. Proteins that were undetected at the expected molecular weight in elution fractions include Calsequestrin and Orai. Out of the three technical replicates, Junctin appears once in the elution fraction at its expected molecular weight with faint intensity. At best, a Xin-Junctin interaction is weak. Positive controls include blotting for Xin and it's known binding partner Filamin C. To verify the CO-IP efficacy, we pulled down a different HA-tagged protein (GST-PI3K-SH2-HA) and detected HA in the elution and flow-through fractions.

Xin interacts with mitochondria related proteins

Detecting mitochondrial associated proteins (VDAC, Mitofusin 1 + 2) in Xin Co-IP fractions resulted in low resolution and poor intensity bands. To overcome these technical barriers, we enriched mitochondria in lysate using a mitochondria isolation kit and performed the Co-IP from crude mitochondrial fractions (*Fig. 16)*. We observed intense bands in elution fractions for mitochondrial proteins VDAC1 and Mitofusin 1, while Mitofusin 2 had a band with significantly fainter intensity. To further validate the finding of Xin (bait) precipitating with VDAC (prey), we reversed the Co-IP functional roles. Co-IP of VDAC (bait) co-immunoprecipitated with Parkin and Xin *(Fig. 17)*. Parkin has been previously shown to interact with VDAC and thus we used this interaction as a positive control for our VDAC Co-IP. Xin was detectable in the VDAC elution fraction albeit with minimal intensity. To validate the binding specificity of the VDAC primary antibody used for this experiment appropriate isotype controls should be used such as a normal rabbit IgG.

Discussion

The first aim of the study was to establish an effective adenoviral infection protocol which overexpressed recombinant Xin and then measure its effects on cell morphology and physiology. We were successful in validating Xin overexpression at proteomic and transcriptomic levels. We then probed for differences in mitochondrial activity, F-actin distribution, myoblast migration, and differentiation between Xin OE cells and control.

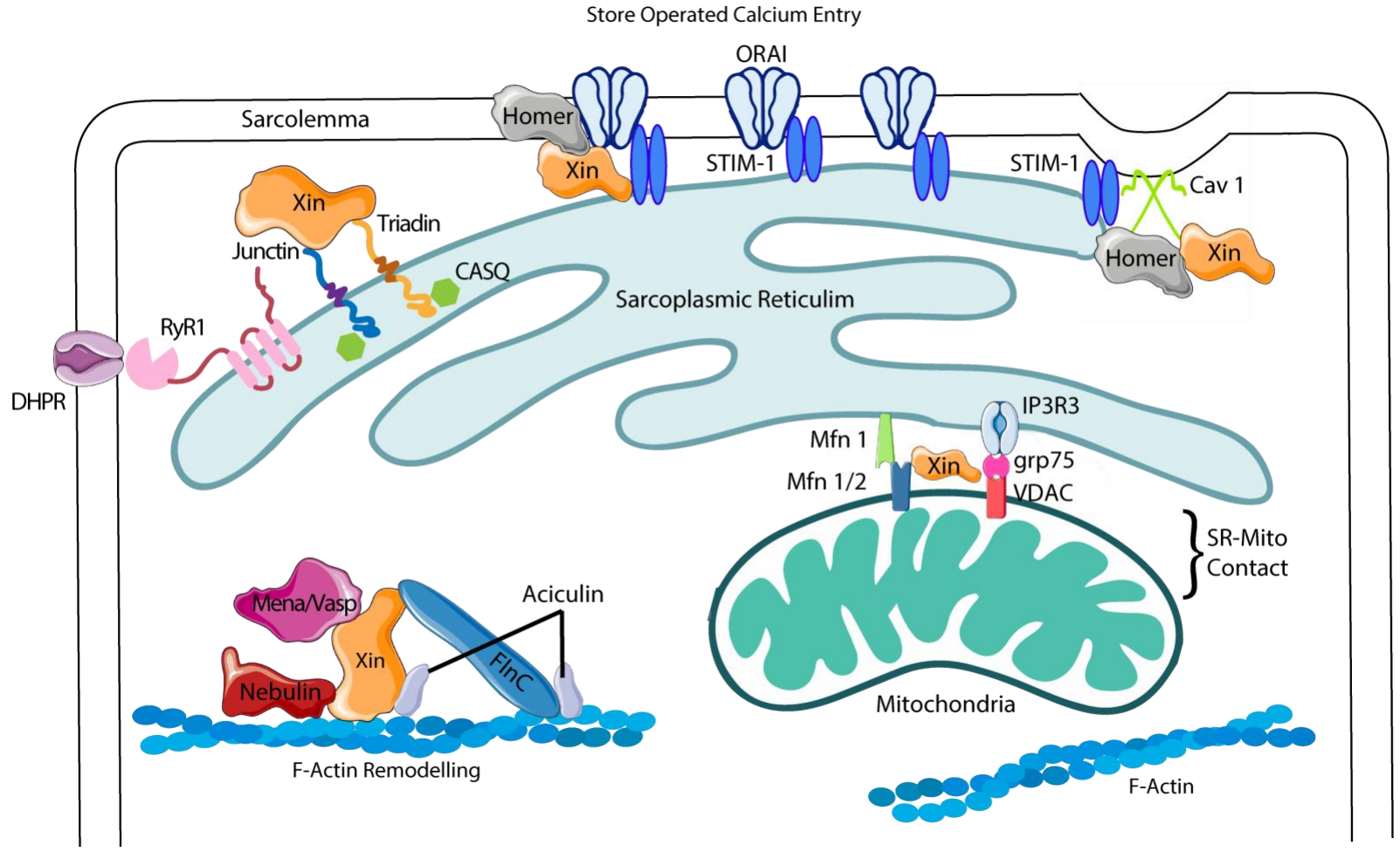

Illustration 6: Xin intracellular protein interactions. Previously known interactions related to F-actin remodeling shown in the bottom left. Proposed interactions related to intracellular calcium handling such as stabilizing Triadin, Junctin, Stim-1, Orai shown. Xin localizes to mitochondria and likely interacts with Mitofusin 1, Mitofusin 2 and VDAC. Xin may also accompany scaffolding protein Homer as it interacts with Cav1 at caveolae regions.

Observing the detriment to cell migration and differentiation when Xin is overexpressed, we sought to understand why. This led to our characterization of Xin's subcellular location and subsequent identification of its various molecular binding partners which may facilitate its proposed physiological functions in calcium signalling and mitochondrial regulation.

Xin OE attenuated normal C2C12 differentiation hallmarked by a shorter myotube length and reduced myotube fusion. Al-sajee et al, previously demonstrated that Xin -/- SCs displayed increased basal activation but reduced proliferation, which was likely the cause of impaired Xin -/- skeletal muscle regeneration following cardiotoxin injury.[56] The impact of Xin OE on myoblast differentiation in the present study resulted in similar outcomes to Xin Knockdown.[56] Meaning that levels of Xin must be fine-tuned for skeletal muscle regeneration to occur. Myoblast migration is a key step in myogenesis and regeneration, as it allows myoblast alignment and their fusion into myotubes.[7,33] The fusion process is known to be Ca^{2+} dependent, and early differentiation is preceded by an increase of cytosolic Ca^{2+} from the extracellular space. [75] For instance, studies in C2C12 cells show the entry of Ca^{2+} through TRPC1 channels, induces transient activation of calpains and subsequent proteolysis of MARCKS, which in turn, allows myoblast migration and fusion.[39] Our lab's experiments have confirmed a functional need for Xin to associate with the macromolecular components of SOCE to allow calcium entry during fatiguing muscle contractions,[57] and we show Xin physically interacts with those components such as Homer, Stim-1, and Orai. Moreover, Homer facilitates a physical interaction with TRPC family members,[76] and its upregulation in expression precedes myotube fusion and thus skeletal muscle differentiation.[43,77] Thus, we propose that Xin's effect to C2C12

motility, fusion, and ultimately differentiation are due, in part, to a destabilization of SOCE components necessary for extracellular Ca^{2+} entry.

It is also important to consider that myogenic differentiation is an energetically demanding process which is largely supported by mitochondrial ATP production, and differentiation is attenuated by a decrease in functional mitochondria.[78] Although we observed no differences in global mitochondrial activity between Xin OE and control cells, we were surprised to note the increased mitochondrial content in Xin OE cells as indicated by increased western blot intensities of mitochondrial oxidative phosphorylation enzymes. This phenomena of the myocytes increasing the number of mitochondria to compensate for individual mitochondria dysfunction is well characterized. [79] For example, the first recognition of this phenomena came from the skeletal muscle of a hypermetabolic patient which contained large numbers of abnormal mitochondria.[80] We observe this compensatory mechanism again in Xin -/- skeletal muscle, as deficits in mitochondrial ETC respiration were only detected when normalized to the increased mitochondrial content.[71] Thus, if Xin OE myoblasts also resulted in mild ETC dysfunction, these changes would likely be invisible to mean MitoTracker intensity per cell, as the cell will compensate with increasing abnormal mitochondria number. Although we were unable to detect individual mitochondrial impairments in Xin OE cells due to our limited methodology, Xin OE cells do share the phenotypic increase in mitochondria number as Xin -/- skeletal muscle, which also had prominent mitochondrial swelling, abnormal cristae, and dysfunction. In the present study, we provide further evidence that supports a physical Xin-

mitochondria interaction. We show that Xin colocalized to mitochondria markers (MitoTracker, COXIV) and is present in mitochondrial subcellular fractionations.

Deficits in myogenic differentiation when Xin is overexpressed have been explained by two different theories; disrupted calcium entry and deficits in mitochondria bioenergetics. These two seemingly separate theories intersect with the postulate that Xin is a MAM tether, or stabilizes other MAM tethers. We show Xin is associated with a cohort of MAM tethering proteins such as Mitofusin1, Mitofusin 2, and VDAC. These MAM tethers essentially juxtapose mitochondria and sarcoplasmic reticulum in skeletal muscle to facilitate efficient calcium transport,[67,63] autophagy[72] and mitochondrial dynamics.[60,61] Structurally, the adaptor protein Xin is likely playing an indirect tethering role by stabilizing the Mitofusin 1/2 tether and IP3R-Grp-VDAC tether complex. Functionally, both of these tether complexes are important for mitochondrial calcium uptake. [81,82] Considering Xin associates with the aforementioned calcium proteins and mitochondrial tethers, localizes to mitochondria, and Xin -/- experiments result in the mislocalization of mitochondria, we suggest that Xin structurally stabilizes MAM tethers for calcium transfer.

Lastly, a recent 2020 study by Holt et al, illustrated an interaction of Popeye domain-containing proteins 1/2 (POPDC 1/2) with Xin in human skeletal myotubes.[83] Interestingly, they suggest caveolin-3 is part of the POPDC1/XIRP1 complex to repair plasma membranes in skeletal muscle, although they were unable to verify this interaction using pulldowns. We instead report a novel Xin caveolin-1 interaction. Caveolin-1 and Caveolin-2 are co-expressed in a variety of

cell types, while caveolin-3 is a muscle-specific isoform.[84] However, Cav-1 and Cav-3 form heterooligomeric complexes in myocytes. [85] In addition, CAV1 has been identified as a hepatic MAM tether protein which regulated intracellular steroid and lipoprotein metabolism-related processes. [70] Therefore, Xin may interact with CAV1 to stabilize a MAM tether complex and/or repair the plasma membrane as a complex with CAV1/CAV3 heterooligomers with POPDC1/2.

Future Directions

While we made significant advances in our understanding of Xin's role(s) within skeletal muscle, future studies are necessary to fully uncover all aspects of Xin's functions. First, whether Xin OE has a direct impact on mitochondrial health can be determined by visualizing mitochondrial number, localization, morphology and testing respiratory function. For instance, measuring mitochondrial oxygen consumption rate at electron transport complexes using Seahorse assays is of interest. The specific role of Xin within MAM tethers should be addressed by measuring SR-Mito contact surface area and distance between Xin -/- and WT muscle tissues, and Xin OE and WT muscles. Second, characterizing Xin overexpression and calcium dynamics should be explored. For example, to determine if Xin OE improves calcium handling or fatigue resistance, we can measure calcium fluxes using Indo-1 during prolonged skeletal muscle contractions.

Lastly, the role of Xin in human development has been largely left unaddressed. Alazami et al, found Xirp1 to be one of 69 candidate recessive genes identified where genetic mutation would lead to encephalopathy.[86] In addition, our unpublished data in collaboration with Genematcher, has identified patients with *Xirp1* mutations who exhibit a variety of phenotypes including

cardiac dysfunction, myotonia, cerebral calcifications, microcephaly and developmental delays. Considering Xin is highly upregulated during ischemia/ reperfusion[87], its scaffolding partner Homer plays a an role in neuronal development[43], and bioinformatic prediction candidates include neuronal proteins Notch-3 and Sushi domain containing protein 5 (SUSD5), the role of Xin in neurons and brain vasculature should be investigated.

Figures

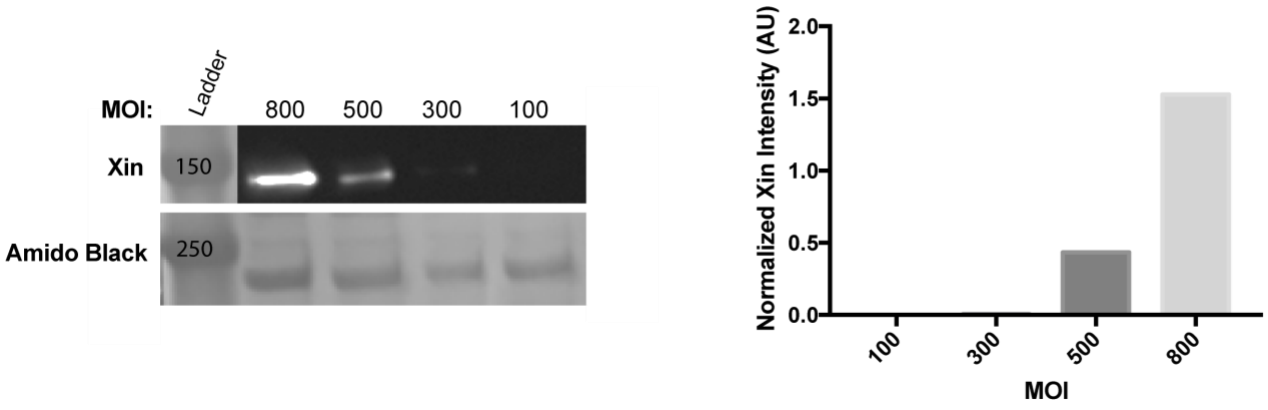

Fig. 1. Protein verification of adenoviral mediated Xin overexpression system in C2C12 myoblasts. Western blot of increasing anti-HA antibody signal associated with increasing viral multiplicity of infection (MOI). Bar graph displays normalized Xin intensity to Amido Black staining.

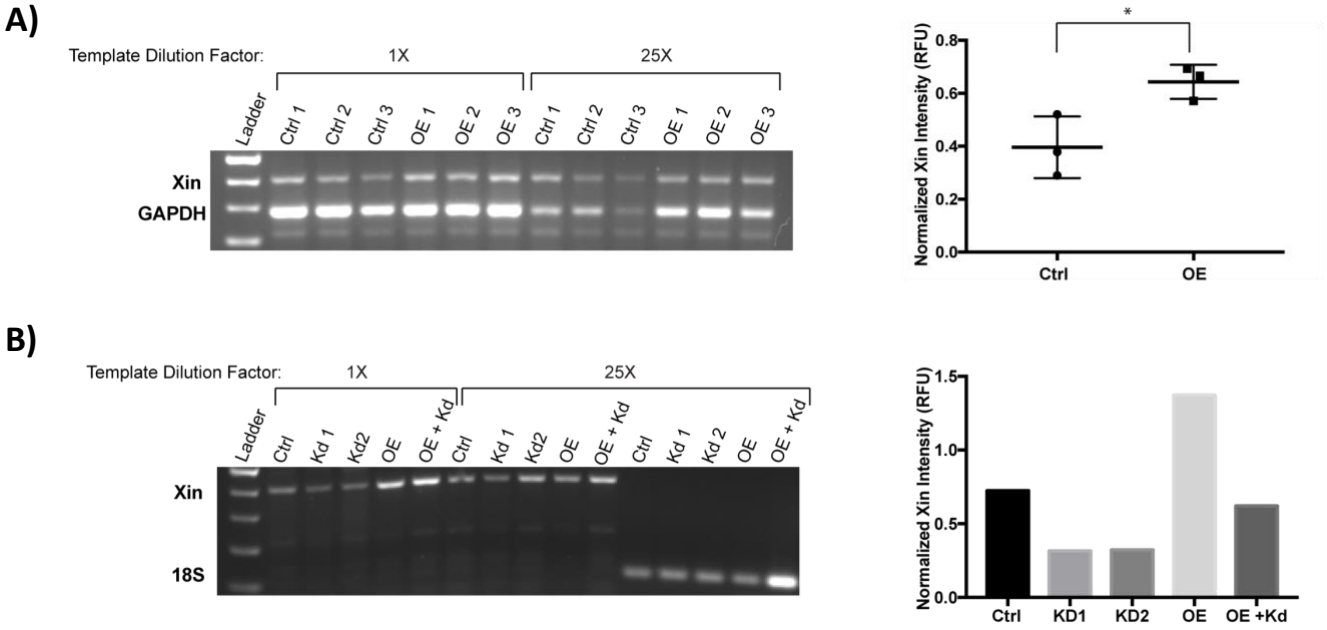

Fig. 2. Transcriptomic verification of adenoviral Xin overexpression system in C2C12 myoblast and primary myoblast cell lines. **A**) Semiquantitative-PCR analysis of reverse transcribed XIRP1 (~400bp) and GAPDH (~300bp) from cDNA of primary myoblasts treated with ADV-HA-Xin and ADV-Null MOI 500, data points of normalized XIRP1 intensities displayed adjacent. Analyzed using unpaired students *t* test (*= p <.05). **B**) Semiquantitative-PCR analysis reverse transcribed XIRP1 (~400bp) and 18S (~300bp) cDNA of C2C12 treated with ADV-HA-Xin, ADV-Null, ADV-Xin siRNA, and both ADV-HA-Xin and ADV-Xin siRNA. Bar graphs of normalized intensity displayed adjacent.

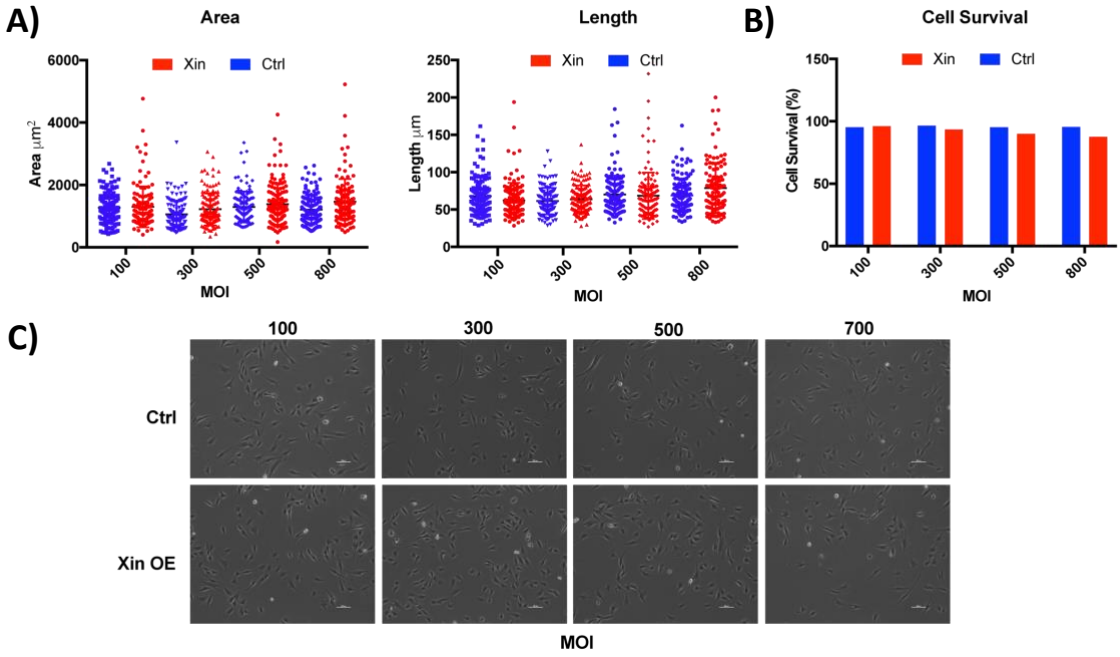

Fig. 3. Effect of Xin overexpression on C2C12 myoblast morphology and survival. No demonstratable differences in average cell area or length (Mean ± St.dev) as MOI increases (N=130) analyzed using a 2 way ANOVA **B)** No major differences in cell survival 40 hours after adenoviral infection, each bar graph represents 1 well (~250 cells counted). Cells were trypsinized and stained with Trypan Blue to assess cell membrane integrity and infer viability. **C)** Representative image, scale bar denotes 100 μm.

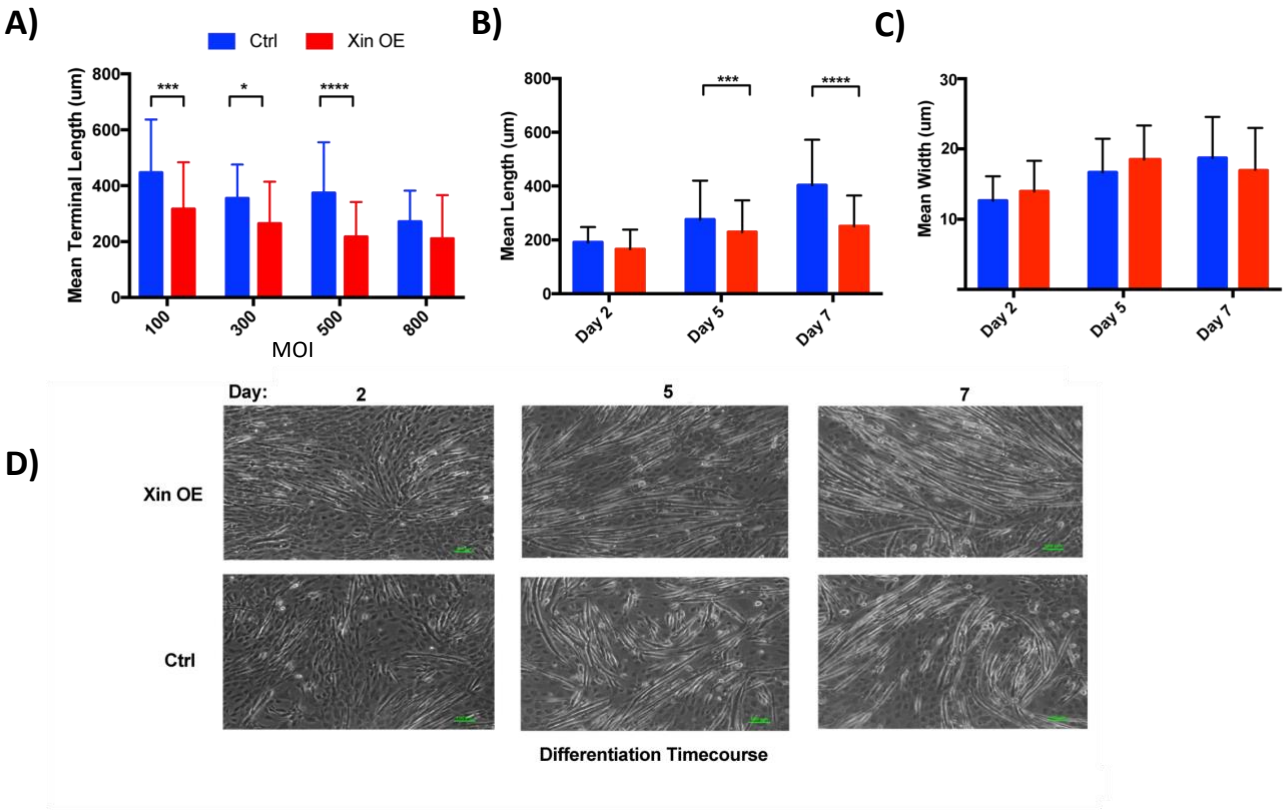

Fig. 4. Effect of Xin overexpression on C2C12 differentiation measuring myotube lengths and widths. **A)** After 2, 5 and 7 days of culture in differentiation media, myotube lengths (µm) and widths (µm) of ADV-HA-Xin infected and control cells were measured. **B)** Xin OE myotube lengths measured at 7 days in differentiation media with increasing MOIs and compared to control (N>100) **C)** Representative images adjacent. Data was analyzed using a 2 Way ANOVA (Time and group effects are significant P<.0001) post hoc multiple comparisons test (*= P<.05, ***= P < .001, **** = P<.0001). Values are Mean ± Standard Deviation (N>80).

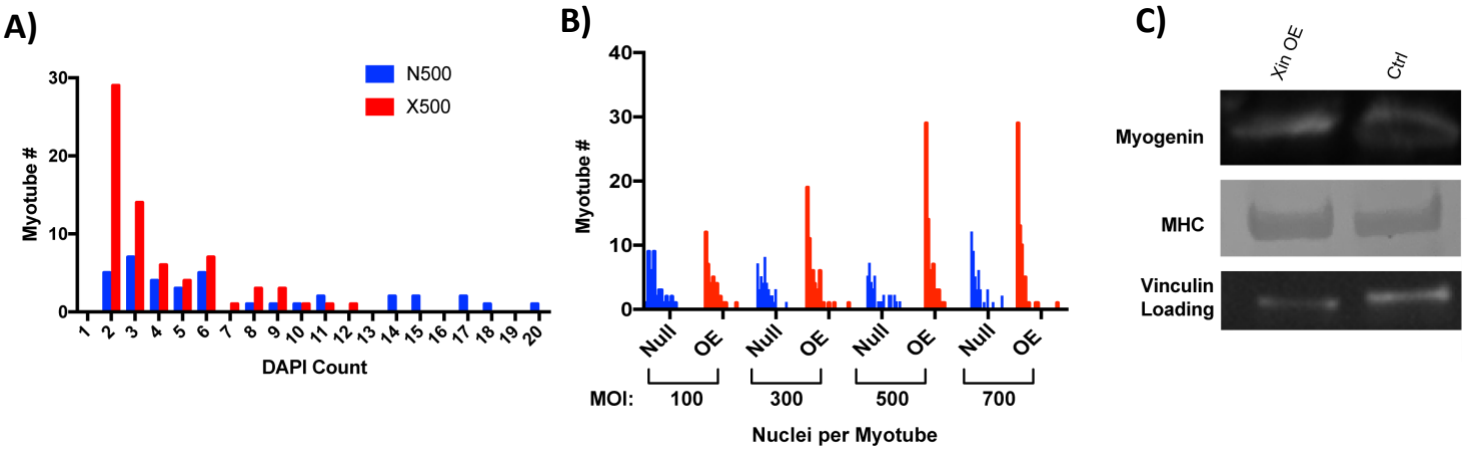

Fig. 5. Characterizing Xin overexpression on C2C12 differentiation measuring nuclear fusion and protein markers. **A)** Distribution overlay of myotube count per nuclei in differentiated C2C12 cells infected with ADV-HA-Xin (Xin OE) and ADV-Null (Control) with multiplicity of infection of 500 (N=50) **B)** Compiled bar graphs of myotube count per increasing nuclei number for differentiated cells infected with ADV-HA-Xin and ADV-Null and Xin OE with increasing multiplicity of infections of 100, 300, 500, 800. **C)** Western blots for terminal differentiation protein markers myosin heavy chain (MHC), Myogenin, and Vinculin as a loading control taken from cell lysates at day 7 of differentiation (N=1).

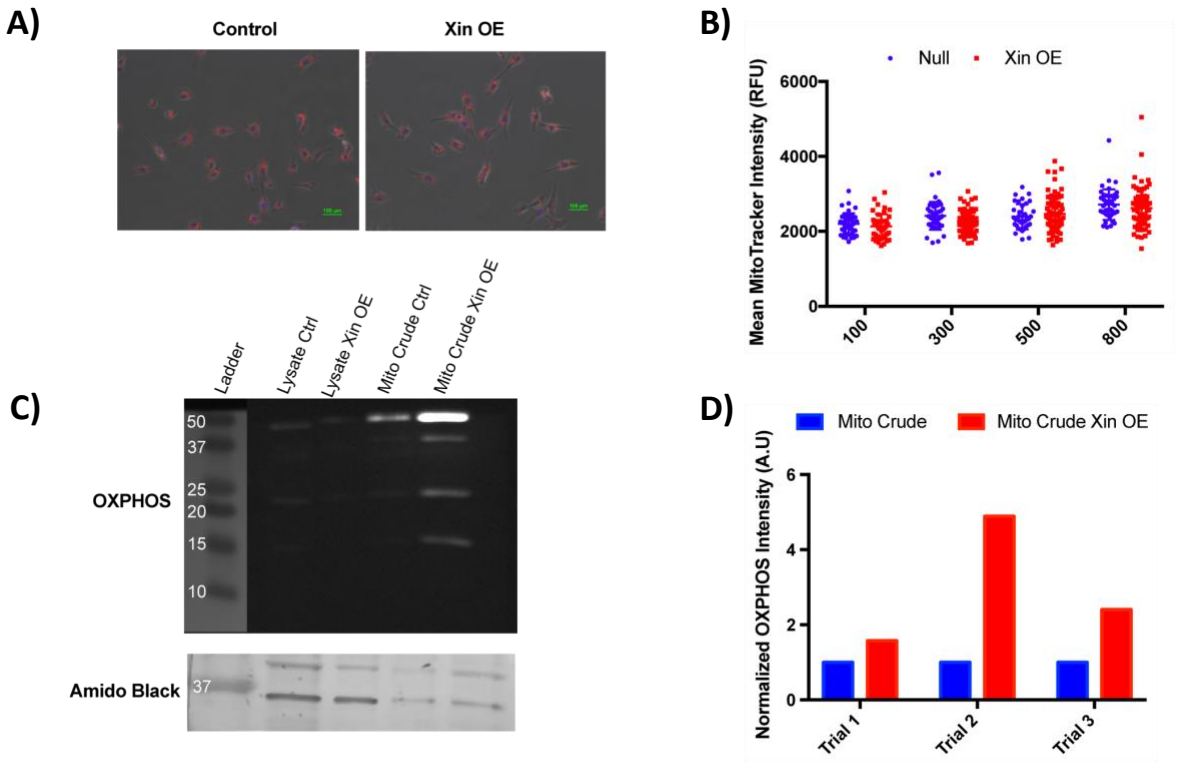

Fig. 6. MitoTracker staining and mitochondria content of Xin overexpression C2C12 cells. **A)** Representative images of Xin OE and control C2C12 myoblasts live cell stain of MitoTracker CMXROS and DAPI. **B)** No differences in mean MitoTracker signal intensity per cell with Xin OE or knockdown compared to control. **C)** Representative image of OXPHOS western blot of mitochondrial isolations and whole cell lysates after Xin overexpression (n=3). **D)** Technical replicates of sum OXPHOS intensity from crude mitochondrial fractions of Xin OE myotubes and control.

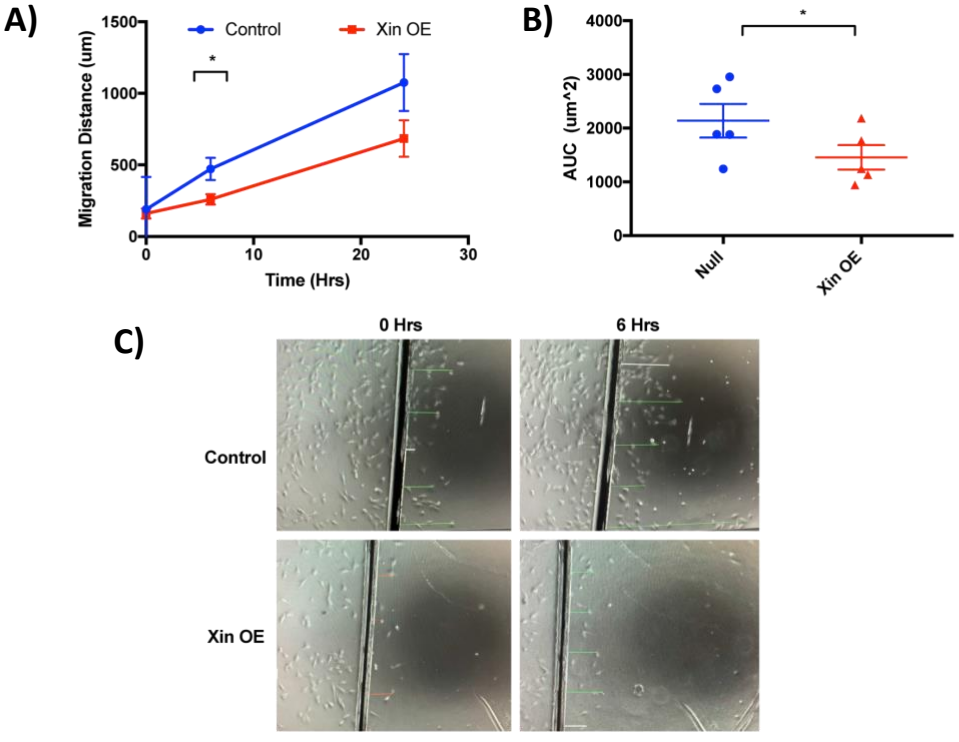

Fig. 7. Scrape assay of C2C12 cells overexpressing Xin. **A)** Time course of average (Mean ± St. Dev) of migration distance of Xin OE cells is shorter compared to control. **B)** Graphical representation of area under curve (Mean ± St. Dev) of migration distance is statistically significant using students unpaired *t* test (* = p<.05). **C)** Visual representation of quantifying cell migration distance using light microscopy techniques.

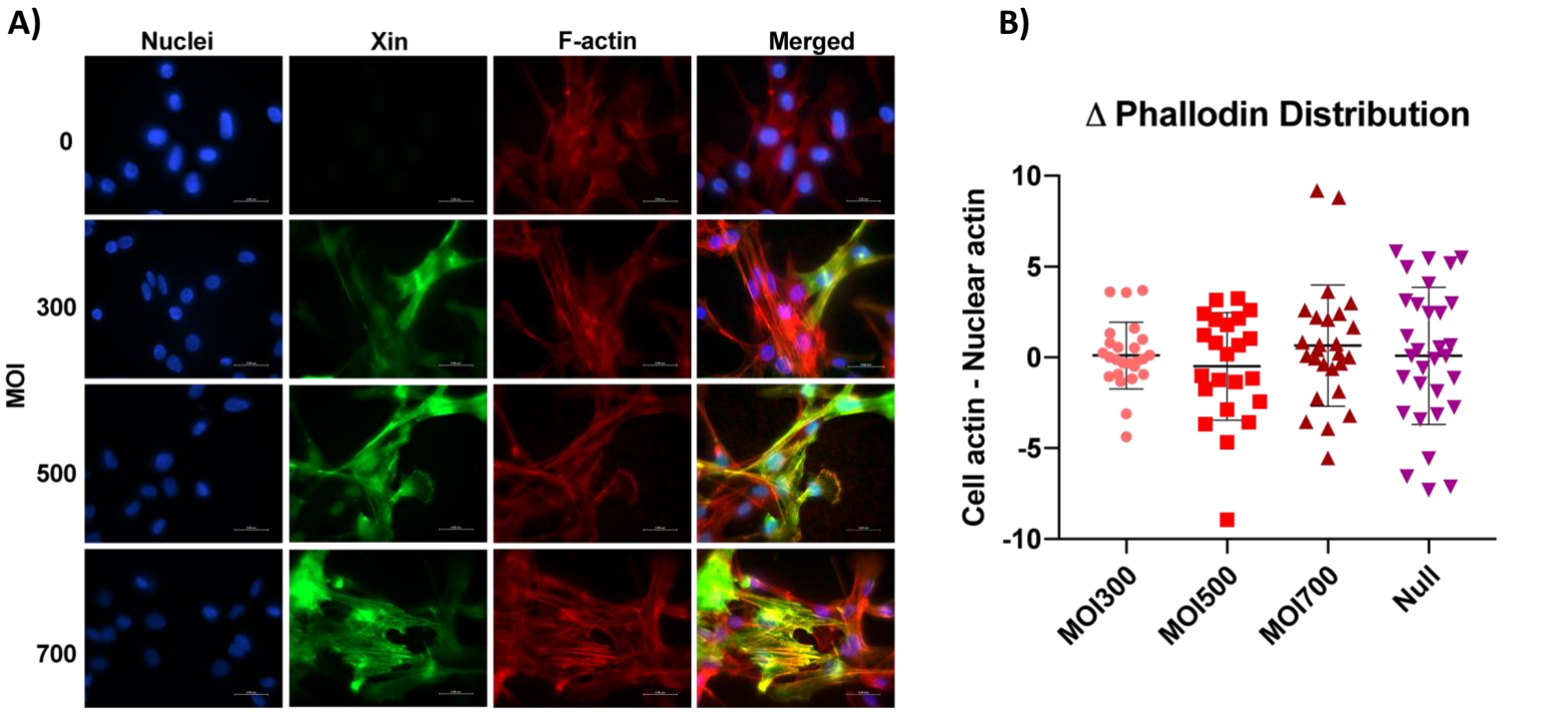

Fig. 8. Xin colocalizes to C2C12 myoblast actin cytoskeleton and does not change actin distribution **A)** Filamentous actin visualized by Alexa fluorescent conjugated phalloidin and Xin visualized by anti-HA immunocytochemistry. No changes in F-actin observed as MOI increases. **B)** Cellular phalloidin distribution analyzed by measuring differences in

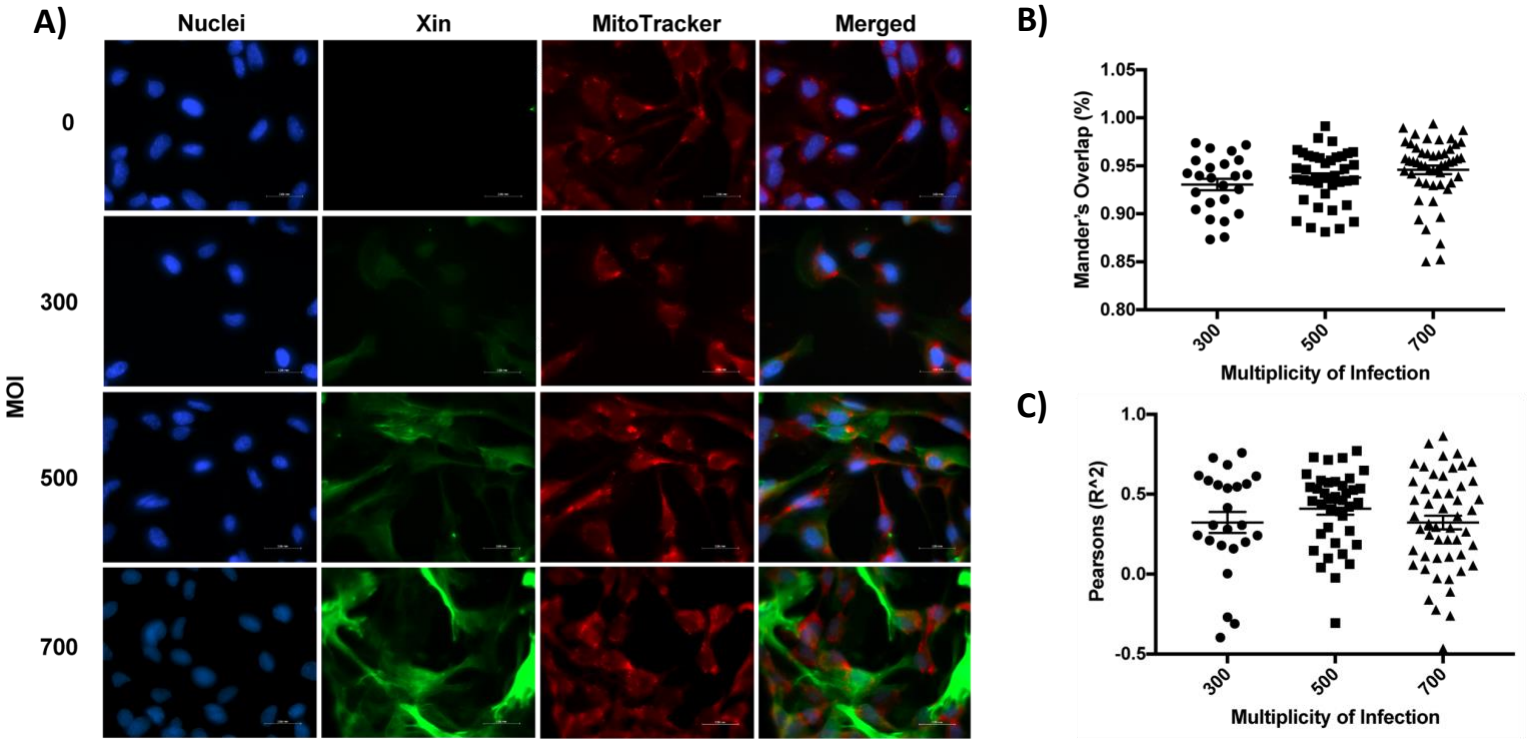

Fig. 9 Xin colocalizes to C2C12 myoblast mitochondria visualized by MitoTracker staining. Ha-Xin overexpressing C2C12 cells stained by anti-HA (green) and MitoTracker (red). Cells infected with increasing MOI and thus increasing quantities of Xin protein. Mander's overlap percentage and Pearson's correlation analysis (n=50) performed using NIS

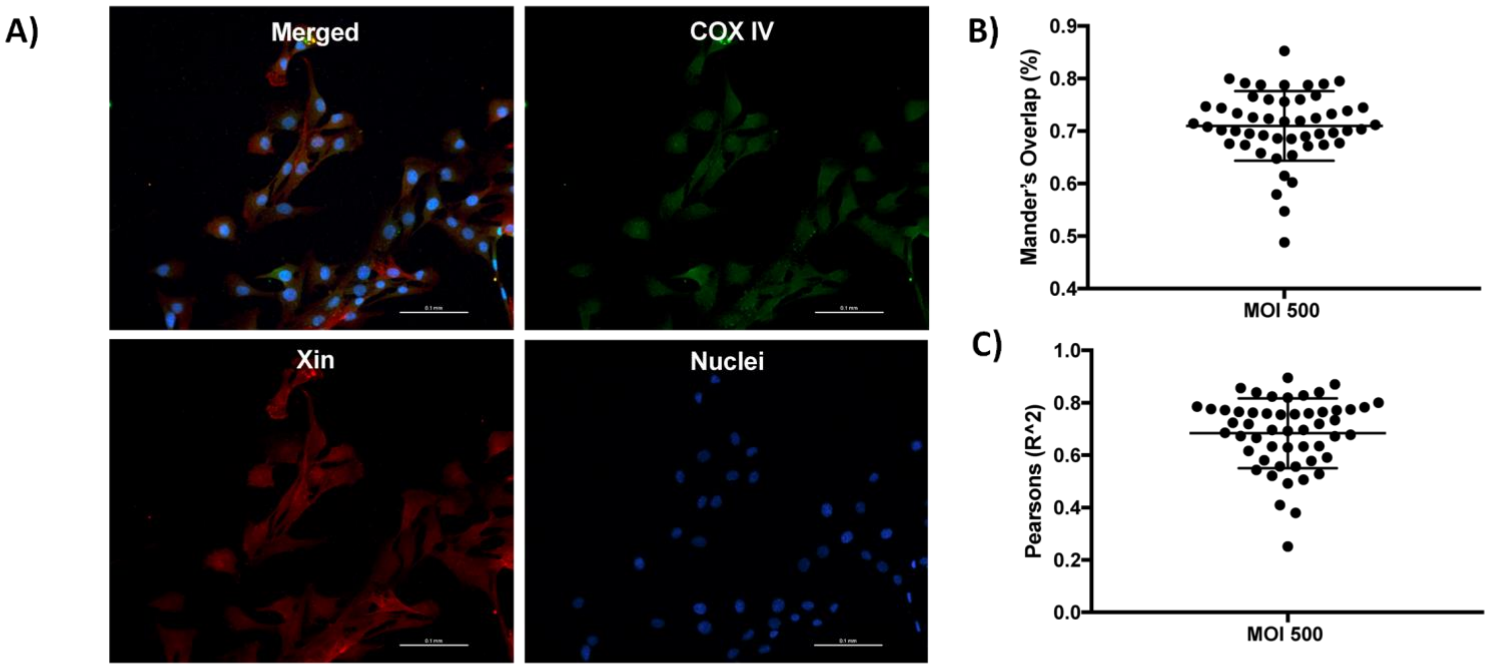

Fig. 10 Xin colocalizes to C2C12 myoblast mitochondria visualized by COXIV staining. Ha-Xin overexpressing C2C12 cells (MOI500) stained by anti-HA (red) and aniti-COXIV (green). Mander's overlap percentage and Pearson's correlation analysis (n=50) performed using NIS elements software. Error bars denote standard deviation.

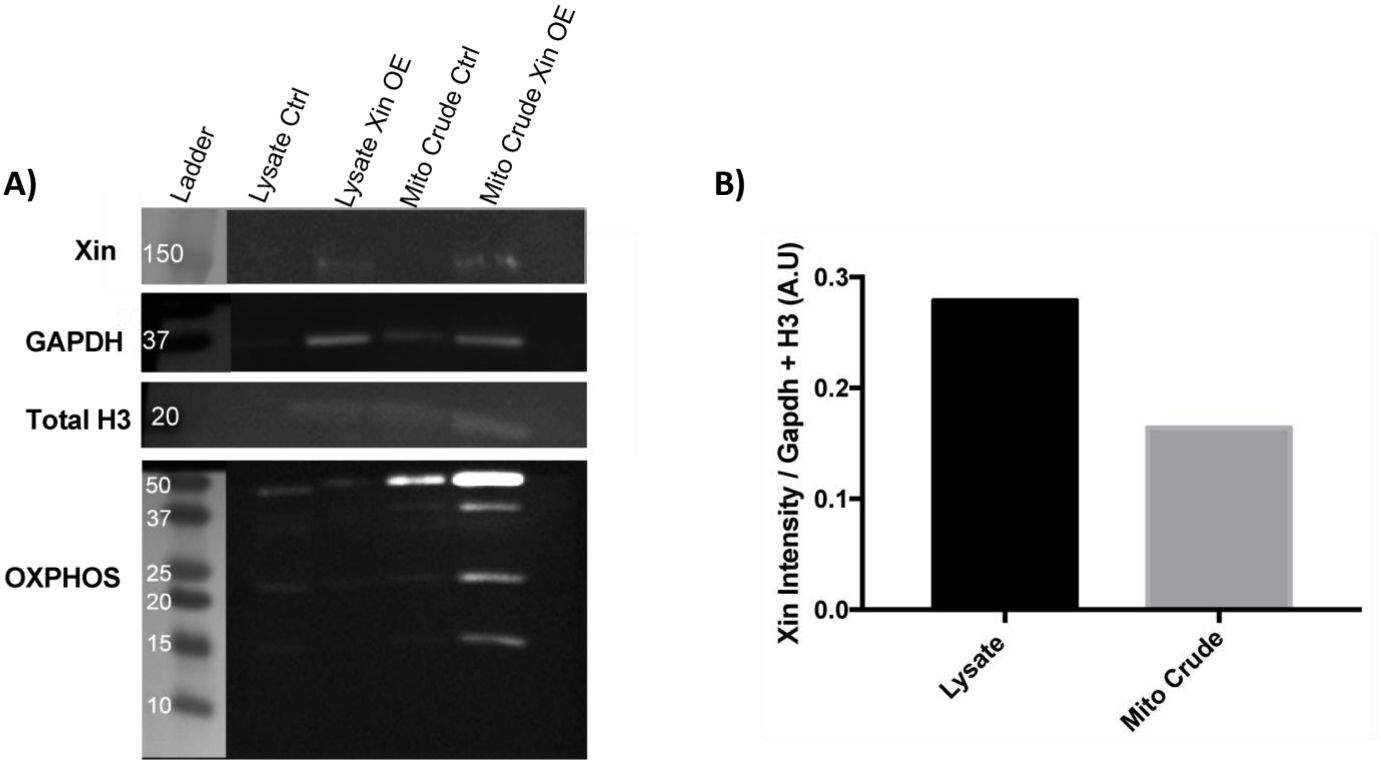

Fig. 11 Xin is present in mitochondrial fractions. Nuclear (total H3), cytoplasmic (Gapdh), and mitochondrial (OXPHOS) markers western blotted to determine purity of the mitochondrial fractionation. Bar graphs displaying Xin intensities normalized to the sum of Gapdh and total histones between lysate and mitochondrial fractions shown adjacent.

A)

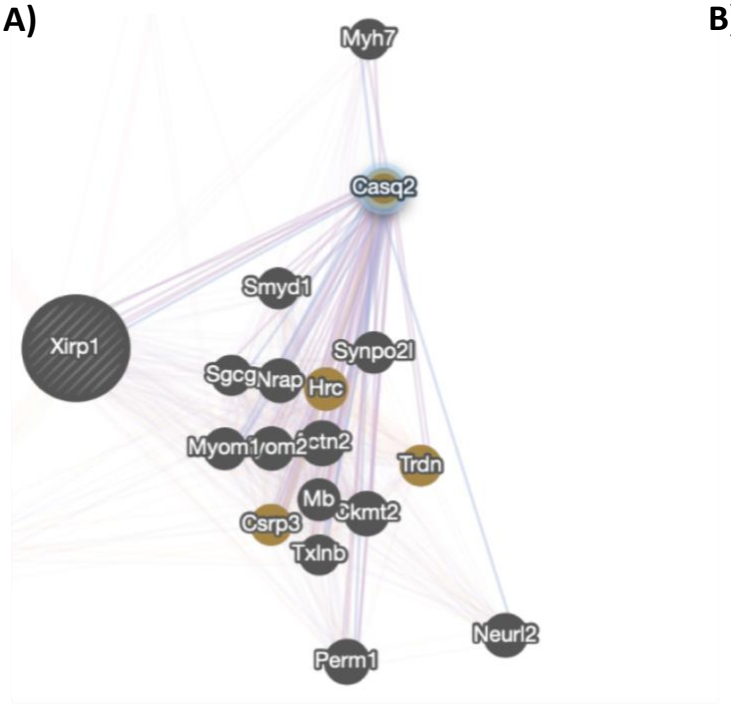

B)

STRING Interaction Network Table

Interactor	Coexpression	Expt Score	Text Score	Total Score
Myom2	0.513	0	0.517	0.755
Flnc	0.167	0.315	0.571	0.734
Nrap	0.417	0.092	0.506	0.716
Myoz	0.594	0	0.309	0.708
Cav3	0.541	0.098	0.306	0.687
Ttn	0.356	0	0.497	0.662
Myom1	0.588	0	0.208	0.66
Oxnad1	0	0	0.647	0.647
Obscn	0.283	0.086	0.494	0.639
Susd5	0.062	0	0.604	0.612
Myl3	0.725	0	0.397	0.544
Actn2	0.36	0.103	0.268	0.543
Tcap	0.226	0	0.275	0.415

Fig. 12. Xirp1 predicted protein interaction networks. **A)** GeneMania network of XIRP1 in *Mus musculus*, evidence of physical interactions in pink, co-expression in purple, co-localization in blue. Interactors with gene ontology categorized under calcium ion homeostasis highlighted in yellow. **B)** Table of functional protein associated STRING network for top 13 interactors with XIRP1 ranked by increasing total score.

A)

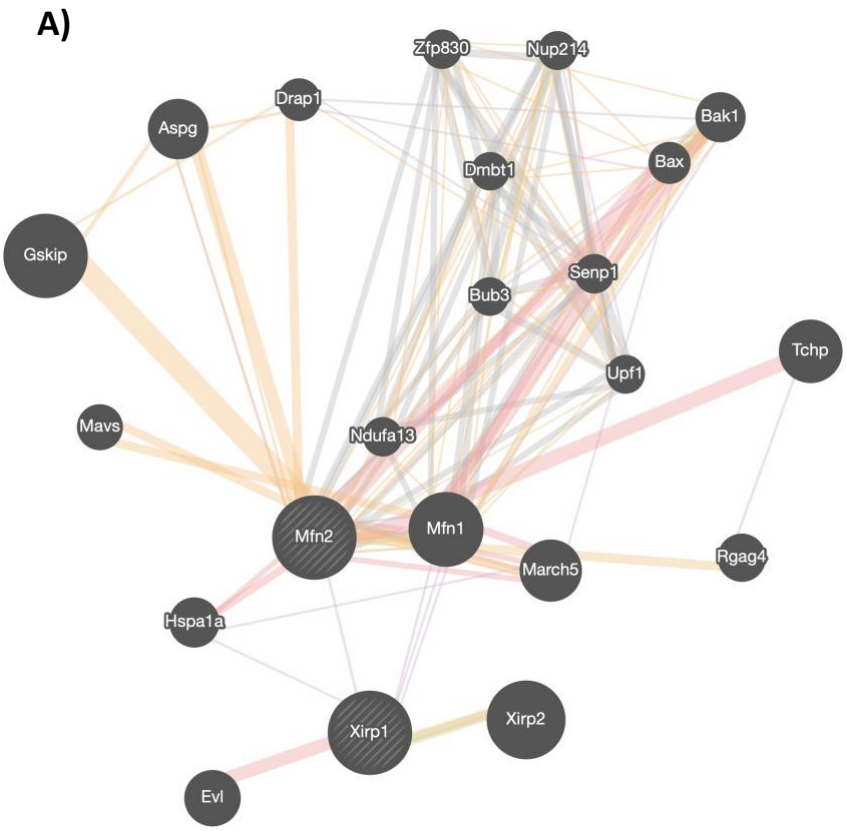

B)

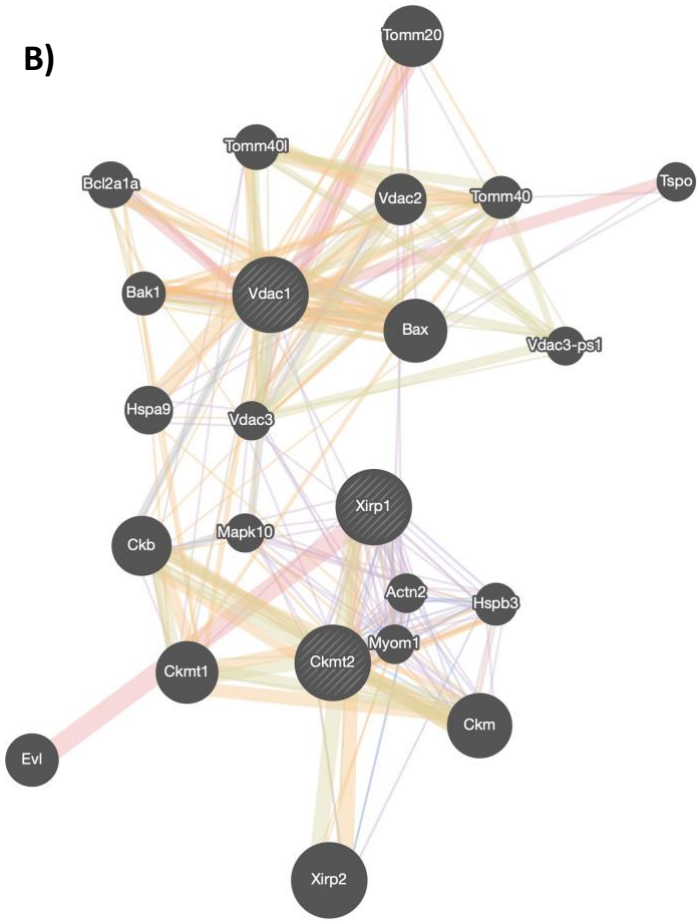

Fig. 13. Xirp1 predicted protein interaction networks in *Mus musculus*. A) GeneMania networks for queries of XIRP1, VDAC1 and CKMT2 B) Xirp1 and Mitofusin 2 query. Physical interactions are coloured pink, co-expression purple, predicted in orange, genetic interactions green, pathway in teal, co-localization in blue, shared protein domains in yellow.

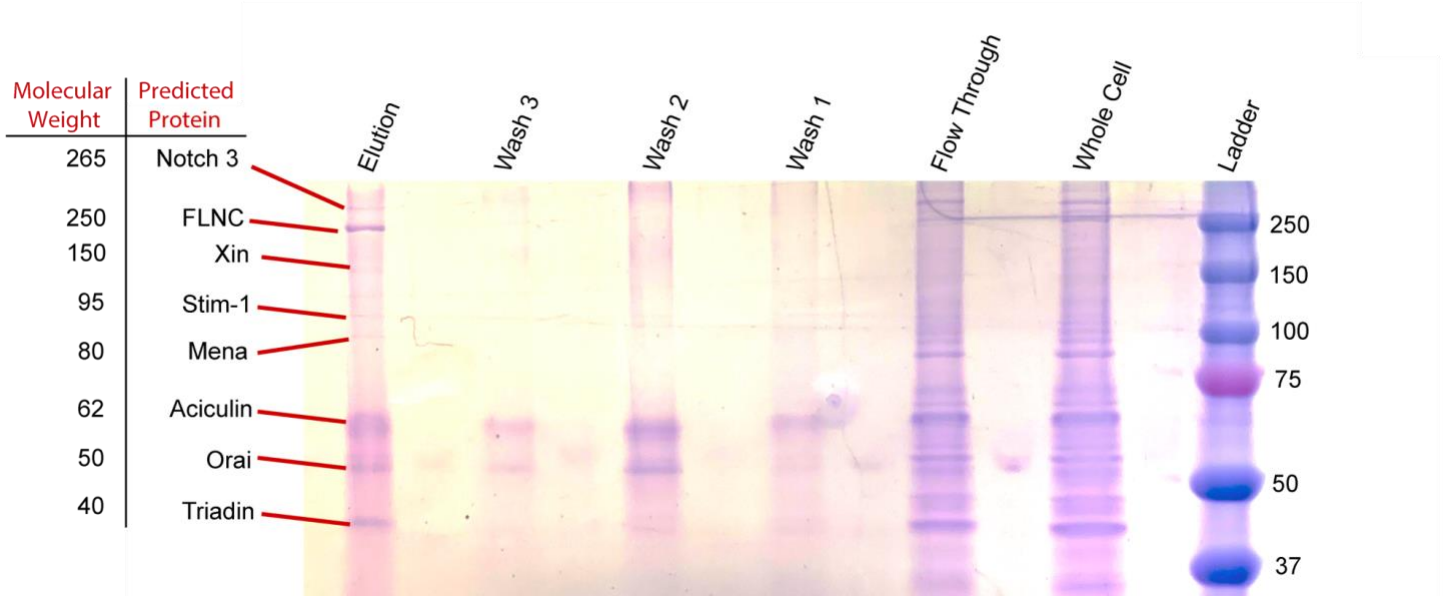

Fig. 14. Coomassie stained 10% gel of HA CO-IP fractions from whole cell lysate of HA-Xin overexpressing C2C12 myotubes. Predicted identities of eluted proteins labelled left to the gel. Predictions based on the molecular weight, known interactions and bioinformatic methods.

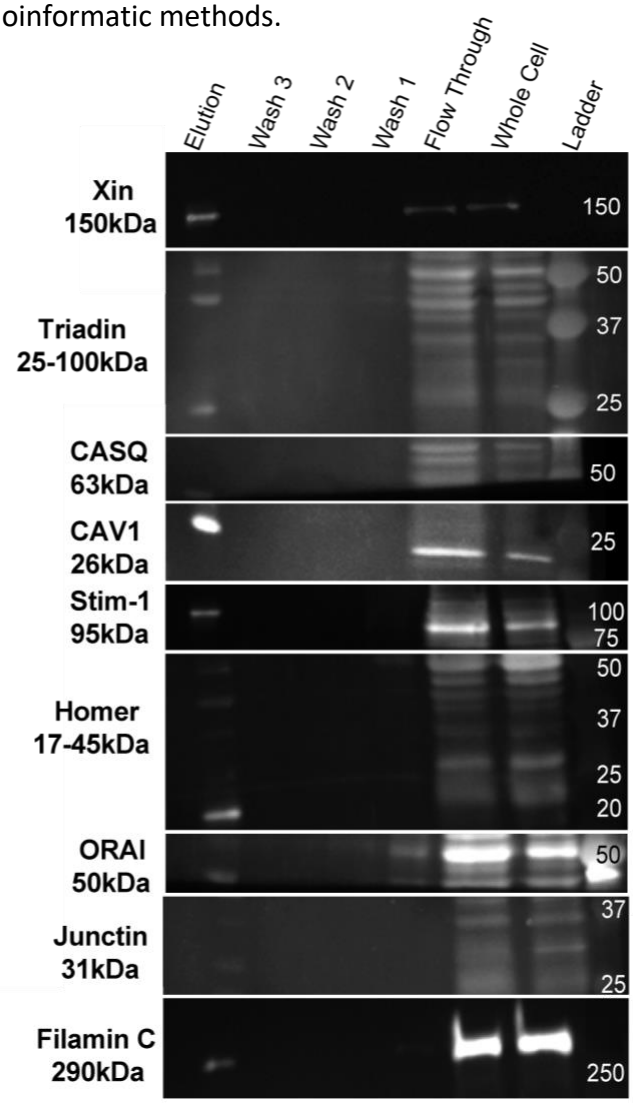

Fig. 15 Western blot analysis of co-immunoprecipitation fractions of Xin OE (+ADV-Xin) differentiated mature myotubes. Calcium related binding partners were assessed. Myotubes infected on day 5 of differentiation and lysed in non-denaturing lysis buffer on day 7. Total of 600ug of protein was immunoprecipitated with anti-HA antibody linked agarose. A representative image of at least 3 independent replicates are shown.

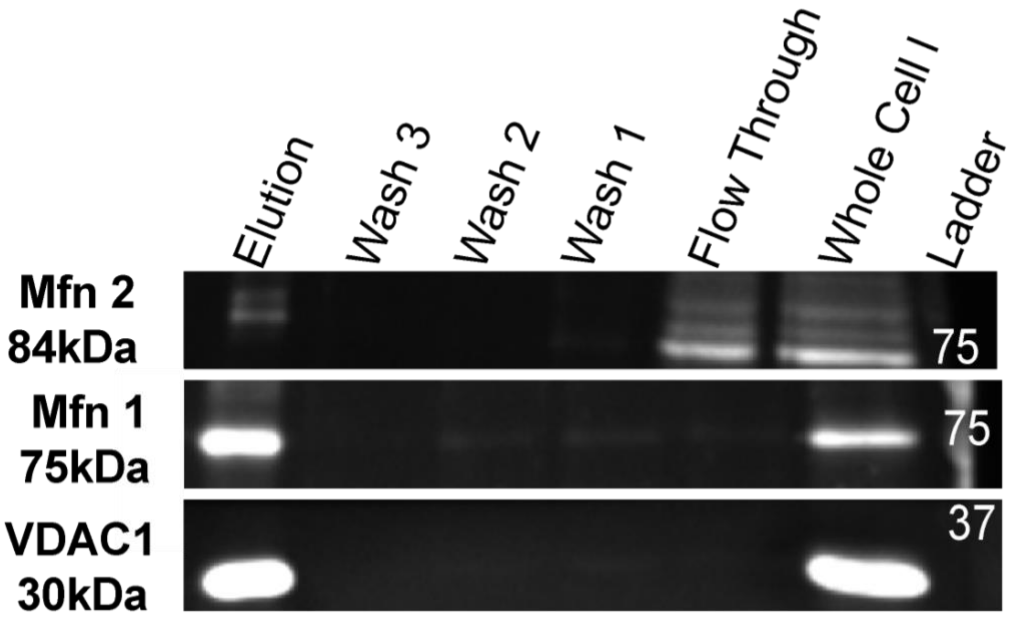

Fig. 16. Western blot analysis of co-immunoprecipitation fractions of Xin OE (+ADV-Xin) from purified mito crude lysate using anti-HA antibody linked agarose. Mitochondrial associated membrane tethering proteins shown

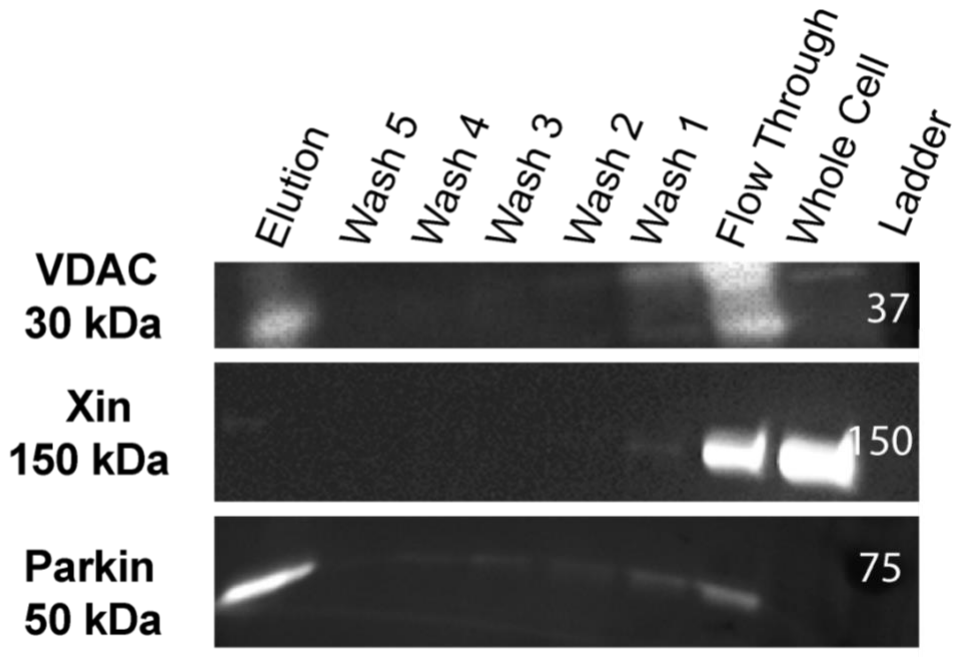

Fig. 17. Western blot analysis of VDAC co-immunoprecipitation from Xin OE cell lysates. VDAC and Parkin are used as positive controls to show the efficacy of pulling down VDAC and published VDAC binding partner Parkin. Immunoblotting for Xin shows strong bands in flow-through and whole cell lanes but a faint band in elution fractions.

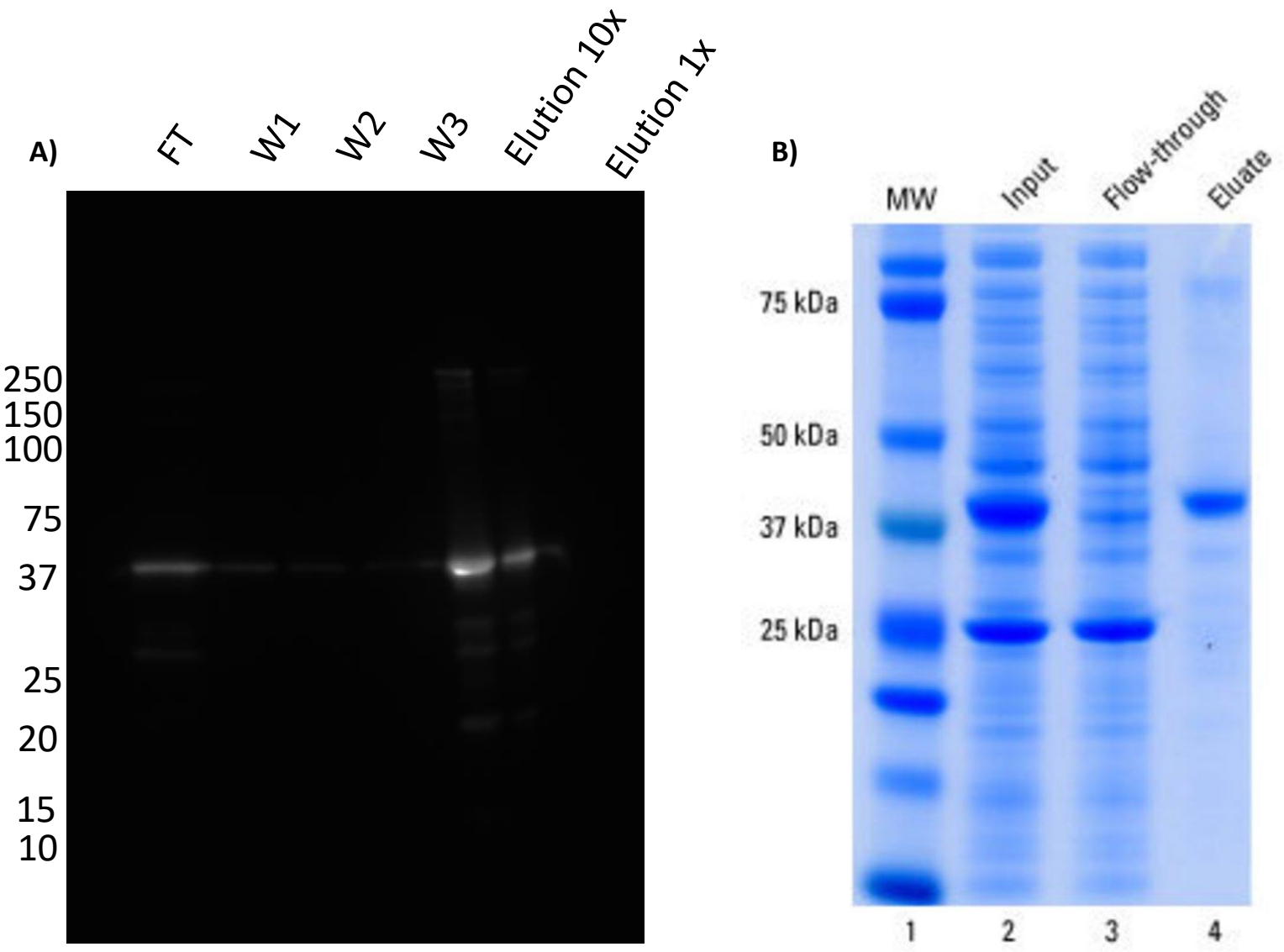

Supplemental 1: Internal control verifying efficacy of HA CO-IP kit. **A)** Anti-HA WB of IP fractions from HA-tagged protein (GST-PI3K-SH2-HA). **B)** IP of HA-tagged protein (GST-PI3K-SH2-HA) analyzed by Coomassie stain (from manufacturer)

References

(1) Tortora, G. J.; Tortora, G. J. *Principles of Anatomy & Physiology, 14th Edition*; 2014.

(2) Grounds, M. D.; White, J. D.; Rosenthal, N.; Bogoyevitch, M. A. The Role of Stem Cells in Skeletal and Cardiac Muscle Repair. *J Histochem Cytochem.* **2002**, *50* (5), 589–610. https://doi.org/10.1177/002215540205000501.

(3) Frontera, W. R.; Ochala, J. Skeletal Muscle: A Brief Review of Structure and Function. *Calcif Tissue Int* **2015**, *96* (3), 183–195. https://doi.org/10.1007/s00223-014-9915-y.

(4) Schultz, E.; McCormick, K. M. Skeletal Muscle Satellite Cells. *Rev. Physiol. Biochem. Pharmacol.* **1994**, *123*, 213–257. https://doi.org/10.1007/bfb0030904.

(5) Liu, J.; Saul, D.; Böker, K. O.; Ernst, J.; Lehman, W.; Schilling, A. F. Current Methods for Skeletal Muscle Tissue Repair and Regeneration. *BioMed Research International* **2018**, *2018*, 1–11. https://doi.org/10.1155/2018/1984879.

(6) van der Meijden, K.; Bravenboer, N.; Dirks, N. F.; Heijboer, A. C.; den Heijer, M.; de Wit, G. M. J.; Offringa, C.; Lips, P.; Jaspers, R. T. Effects of 1,25(OH)2D3 and 25(OH)D3 on C2C12 Myoblast Proliferation, Differentiation, and Myotube Hypertrophy. *J Cell Physiol* **2016**, *231* (11), 2517–2528. https://doi.org/10.1002/jcp.25388.

(7) Yin, H.; Price, F.; Rudnicki, M. A. Satellite Cells and the Muscle Stem Cell Niche. *Physiological Reviews* **2013**, *93* (1), 23–67. https://doi.org/10.1152/physrev.00043.2011.

(8) Murphy, M. M.; Lawson, J. A.; Mathew, S. J.; Hutcheson, D. A.; Kardon, G. Satellite Cells, Connective Tissue Fibroblasts and Their Interactions Are Crucial for Muscle Regeneration. *Development* **2011**, *138* (17), 3625–3637. https://doi.org/10.1242/dev.064162.

(9) Kääriäinen, M.; Järvinen, T.; Järvinen, M.; Rantanen, J.; Kalimo, H. Relation between Myofibers and Connective Tissue during Muscle Injury Repair: Myofiber and Connective Tissue Relationship. *Scandinavian Journal of Medicine & Science in Sports* **2000**, *10* (6), 332–337. https://doi.org/10.1034/j.1600-0838.2000.010006332.x.

(10) Cornelison, D. D. W. Context Matters: In Vivo and in Vitro Influences on Muscle Satellite Cell Activity. *J. Cell. Biochem.* **2008**, *105* (3), 663–669. https://doi.org/10.1002/jcb.21892.

(11) Huard, J.; Li, Y.; Fu, F. H. Muscle Injuries and Repair: Current Trends in Research. *J Bone Joint Surg Am* **2002**, *84* (5), 822–832.

(12) Henderson, C. A.; Gomez, C. G.; Novak, S. M.; Mi-Mi, L.; Gregorio, C. C. Overview of the Muscle Cytoskeleton. In *Comprehensive Physiology*; Terjung, R., Ed.; John Wiley & Sons, Inc.: Hoboken, NJ, USA, 2017; pp 891–944. https://doi.org/10.1002/cphy.c160033.

(13) Ono, S. Dynamic Regulation of Sarcomeric Actin Filaments in Striated Muscle. *Cytoskeleton* **2010**, *67* (11), 677–692. https://doi.org/10.1002/cm.20476.

(14) Guerin, C. M.; Kramer, S. G. Cytoskeletal Remodeling during Myotube Assembly and Guidance: Coordinating the Actin and Microtubule Networks. *Communicative & Integrative Biology* **2009**, *2* (5), 452–457. https://doi.org/10.4161/cib.2.5.9158.

(15) Paulin, D.; Li, Z. Desmin: A Major Intermediate Filament Protein Essential for the Structural Integrity and Function of Muscle. *Experimental Cell Research* **2004**, *301* (1), 1–7. https://doi.org/10.1016/j.yexcr.2004.08.004.

(16) Becker, R.; Leone, M.; Engel, F. Microtubule Organization in Striated Muscle Cells. *Cells* **2020**, *9* (6), 1395. https://doi.org/10.3390/cells9061395.

(17) Pathak, D.; Sepp, K. J.; Hollenbeck, P. J. Evidence That Myosin Activity Opposes Microtubule-Based Axonal Transport of Mitochondria. *Journal of Neuroscience* **2010**, *30* (26), 8984–8992. https://doi.org/10.1523/JNEUROSCI.1621-10.2010.
(18) Molt, S.; Buhrdel, J. B.; Yakovlev, S.; Schein, P.; Orfanos, Z.; Kirfel, G.; Winter, L.; Wiche, G.; van der Ven, P. F. M.; Rottbauer, W.; Just, S.; Belkin, A. M.; Furst, D. O. Aciculin Interacts with Filamin C and Xin and Is Essential for Myofibril Assembly, Remodeling and Maintenance. *Journal of Cell Science* **2014**, *127* (16), 3578–3592. https://doi.org/10.1242/jcs.152157.
(19) The development of the myotendinous junction. A review https://www.ncbi.nlm.nih.gov/pmc/articles/PMC3666507/ (accessed 2020 -01 -06).
(20) Sharafi, B.; Ames, E. G.; Holmes, J. W.; Blemker, S. S. Strains at the Myotendinous Junction Predicted by a Micromechanical Model. *Journal of Biomechanics* **2011**, *44* (16), 2795–2801. https://doi.org/10.1016/j.jbiomech.2011.08.025.
(21) de Palma, L.; Marinelli, M.; Pavan, M.; Bertoni-Freddari, C. Involvement of the Muscle-Tendon Junction in Skeletal Muscle Atrophy: An Ultrastructural Study. *Rom J Morphol Embryol* **2011**, *52* (1), 105–109.
(22) Gerthoffer, W. T. Actin Cytoskeletal Dynamics in Smooth Muscle Contraction. *Can. J. Physiol. Pharmacol.* **2005**, *83* (10), 851–856. https://doi.org/10.1139/y05-088.
(23) Pappas, C. T.; Bliss, K. T.; Zieseniss, A.; Gregorio, C. C. The Nebulin Family: An Actin Support Group. *Trends in Cell Biology* **2011**, *21* (1), 29–37. https://doi.org/10.1016/j.tcb.2010.09.005.
(24) Weber, A.; Pennise, C. R.; Babcock, G. G.; Fowler, V. M. Tropomodulin Caps the Pointed Ends of Actin Filaments. *The Journal of Cell Biology* **1994**, *127* (6), 1627–1635. https://doi.org/10.1083/jcb.127.6.1627.
(25) van der Ven, P. F. M.; Ehler, E.; Vakeel, P.; Eulitz, S.; Schenk, J. A.; Milting, H.; Micheel, B.; Fürst, D. O. Unusual Splicing Events Result in Distinct Xin Isoforms That Associate Differentially with Filamin c and Mena/VASP. *Experimental Cell Research* **2006**, *312* (11), 2154–2167. https://doi.org/10.1016/j.yexcr.2006.03.015.
(26) Pantaloni, D.; Carlier, M.-F. How Profilin Promotes Actin Filament Assembly in the Presence of Thymosin B4. *Cell* **1993**, *75* (5), 1007–1014. https://doi.org/10.1016/0092-8674(93)90544-Z.
(27) Svitkina, T. The Actin Cytoskeleton and Actin-Based Motility. *Cold Spring Harb Perspect Biol* **2018**, *10* (1), a018267. https://doi.org/10.1101/cshperspect.a018267.
(28) Semenova, I.; Burakov, A.; Berardone, N.; Zaliapin, I.; Slepchenko, B.; Svitkina, T.; Kashina, A.; Rodionov, V. Actin Dynamics Is Essential for Myosin-Based Transport of Membrane Organelles. *Current Biology* **2008**, *18* (20), 1581–1586. https://doi.org/10.1016/j.cub.2008.08.070.
(29) Quintero, O. A.; DiVito, M. M.; Adikes, R. C.; Kortan, M. B.; Case, L. B.; Lier, A. J.; Panaretos, N. S.; Slater, S. Q.; Rengarajan, M.; Feliu, M.; Cheney, R. E. Human Myo19 Is a Novel Myosin That Associates with Mitochondria. *Current Biology* **2009**, *19* (23), 2008–2013. https://doi.org/10.1016/j.cub.2009.10.026.
(30) Li, S.; Xu, S.; Roelofs, B. A.; Boyman, L.; Lederer, W. J.; Sesaki, H.; Karbowski, M. Transient Assembly of F-Actin on the Outer Mitochondrial Membrane Contributes to Mitochondrial

Fission. *The Journal of Cell Biology* **2015**, *208* (1), 109–123. https://doi.org/10.1083/jcb.201404050.
(31) Boldogh, I. R.; Pon, L. A. Mitochondria on the Move. *Trends in Cell Biology* **2007**, *17* (10), 502–510. https://doi.org/10.1016/j.tcb.2007.07.008.
(32) Costa, M. L. Cytoskeleton and Adhesion in Myogenesis. *ISRN Developmental Biology* **2014**, *2014*, 1–15. https://doi.org/10.1155/2014/713631.
(33) Sens, K. L.; Zhang, S.; Jin, P.; Duan, R.; Zhang, G.; Luo, F.; Parachini, L.; Chen, E. H. An Invasive Podosome-like Structure Promotes Fusion Pore Formation during Myoblast Fusion. *Journal of Cell Biology* **2010**, *191* (5), 1013–1027. https://doi.org/10.1083/jcb.201006006.
(34) Araya, R.; Liberona, J. L.; Cárdenas, J. C.; Riveros, N.; Estrada, M.; Powell, J. A.; Carrasco, M. A.; Jaimovich, E. Dihydropyridine Receptors as Voltage Sensors for a Depolarization-Evoked, IP3R-Mediated, Slow Calcium Signal in Skeletal Muscle Cells. *Journal of General Physiology* **2003**, *121* (1), 3–16. https://doi.org/10.1085/jgp.20028671.
(35) Periasamy, M.; Kalyanasundaram, A. SERCA Pump Isoforms: Their Role in Calcium Transport and Disease. *Muscle Nerve* **2007**, *35* (4), 430–442. https://doi.org/10.1002/mus.20745.
(36) Wang, Q.; Michalak, M. Calsequestrin. Structure, Function, and Evolution. *Cell Calcium* **2020**, *90*, 102242. https://doi.org/10.1016/j.ceca.2020.102242.
(37) Carrell, E. M.; Coppola, A. R.; McBride, H. J.; Dirksen, R. T. Orai1 Enhances Muscle Endurance by Promoting Fatigue-resistant Type I Fiber Content but Not through Acute Store-operated Ca^{2+} Entry. *FASEB j.* **2016**, *30* (12), 4109–4119. https://doi.org/10.1096/fj.201600621R.
(38) Cho, C.-H.; Woo, J. S.; Perez, C. F.; Lee, E. H. A Focus on Extracellular Ca2+ Entry into Skeletal Muscle. *Exp Mol Med* **2017**, *49* (9), e378–e378. https://doi.org/10.1038/emm.2017.208.
(39) Louis, M.; Zanou, N.; Van Schoor, M.; Gailly, P. TRPC1 Regulates Skeletal Myoblast Migration and Differentiation. *Journal of Cell Science* **2008**, *121* (23), 3951–3959. https://doi.org/10.1242/jcs.037218.
(40) Mazères, G.; Leloup, L.; Daury, L.; Cottin, P.; Brustis, J.-J. Myoblast Attachment and Spreading Are Regulated by Different Patterns by Ubiquitous Calpains. *Cell Motil. Cytoskeleton* **2006**, *63* (4), 193–207. https://doi.org/10.1002/cm.20116.
(41) Dulong, S.; Goudenege, S.; Vuillier-Devillers, K.; Manenti, S.; Poussard, S.; Cottin, P. Myristoylated Alanine-Rich C Kinase Substrate (MARCKS) Is Involved in Myoblast Fusion through Its Regulation by Protein Kinase Cα and Calpain Proteolytic Cleavage. *Biochemical Journal* **2004**, *382* (3), 1015–1023. https://doi.org/10.1042/BJ20040347.
(42) Kim, J. Y.; Zeng, W.; Kiselyov, K.; Yuan, J. P.; Dehoff, M. H.; Mikoshiba, K.; Worley, P. F.; Muallem, S. Homer 1 Mediates Store- and Inositol 1,4,5-Trisphosphate Receptor-Dependent Translocation and Retrieval of TRPC3 to the Plasma Membrane. *Journal of Biological Chemistry* **2006**, *281* (43), 32540–32549. https://doi.org/10.1074/jbc.M602496200.
(43) Salanova, M.; Volpe, P.; Blottner, D. Homer Protein Family Regulation in Skeletal Muscle and Neuromuscular Adaptation: Homer Protein Family Regulation. *IUBMB Life* **2013**, *65* (9), 769–776. https://doi.org/10.1002/iub.1198.

(44) Wang, Y.; Deng, X.; Mancarella, S.; Hendron, E.; Eguchi, S.; Soboloff, J.; Tang, X. D.; Gill, D. L. The Calcium Store Sensor, STIM1, Reciprocally Controls Orai and CaV1.2 Channels. *Science* **2010**, *330* (6000), 105–109. https://doi.org/10.1126/science.1191086.

(45) Dionisio, N.; Smani, T.; Woodard, G. E.; Castellano, A.; Salido, G. M.; Rosado, J. A. Homer Proteins Mediate the Interaction between STIM1 and Cav1.2 Channels. *Biochimica et Biophysica Acta (BBA) - Molecular Cell Research* **2015**, *1853* (5), 1145–1153. https://doi.org/10.1016/j.bbamcr.2015.02.014.

(46) Wang, D. Z.; Reiter, R. S.; Lin, J. L.; Wang, Q.; Williams, H. S.; Krob, S. L.; Schultheiss, T. M.; Evans, S.; Lin, J. J. Requirement of a Novel Gene, Xin, in Cardiac Morphogenesis. *Development* **1999**, *126* (6), 1281–1294.

(47) Otten, J.; van der Ven, P. F. M.; Vakeel, P.; Eulitz, S.; Kirfel, G.; Brandau, O.; Boesl, M.; Schrickel, J. W.; Linhart, M.; Hayeß, K.; Naya, F. J.; Milting, H.; Meyer, R.; Fürst, D. O. Complete Loss of Murine Xin Results in a Mild Cardiac Phenotype with Altered Distribution of Intercalated Discs. *Cardiovascular Research* **2010**, *85* (4), 739–750. https://doi.org/10.1093/cvr/cvp345.

(48) Eulitz, S.; Sauer, F.; Pelissier, M.-C.; Boisguerin, P.; Molt, S.; Schuld, J.; Orfanos, Z.; Kley, R. A.; Volkmer, R.; Wilmanns, M.; Kirfel, G.; van der Ven, P. F. M.; Fürst, D. O. Identification of Xin-Repeat Proteins as Novel Ligands of the SH3 Domains of Nebulin and Nebulette and Analysis of Their Interaction during Myofibril Formation and Remodeling. *MBoC* **2013**, *24* (20), 3215–3226. https://doi.org/10.1091/mbc.e13-04-0202.

(49) Koch, C.; Anderson, D.; Moran, M.; Ellis, C.; Pawson, T. SH2 and SH3 Domains: Elements That Control Interactions of Cytoplasmic Signaling Proteins. *Science* **1991**, *252* (5006), 668–674. https://doi.org/10.1126/science.1708916.

(50) Hawke, T. J.; Atkinson, D. J.; Kanatous, S. B.; Van der Ven, P. F. M.; Goetsch, S. C.; Garry, D. J. Xin, an Actin Binding Protein, Is Expressed within Muscle Satellite Cells and Newly Regenerated Skeletal Muscle Fibers. *American Journal of Physiology-Cell Physiology* **2007**, *293* (5), C1636–C1644. https://doi.org/10.1152/ajpcell.00124.2007.

(51) Sinn, H. W.; Balsamo, J.; Lilien, J.; Lin, J. J.-C. Localization of the Novel Xin Protein to the Adherens Junction Complex in Cardiac and Skeletal Muscle during Development. *Dev. Dyn.* **2002**, *225* (1), 1–13. https://doi.org/10.1002/dvdy.10131.

(52) Feng, H.-Z.; Wang, Q.; Reiter, R. S.; Lin, J. L.-C.; Lin, J. J.-C.; Jin, J.-P. Localization and Function of Xinα in Mouse Skeletal Muscle. *American Journal of Physiology-Cell Physiology* **2013**, *304* (10), C1002–C1012. https://doi.org/10.1152/ajpcell.00005.2013.

(53) Tidball, J. G. Force Transmission across Muscle Cell Membranes. *Journal of Biomechanics* **1991**, *24*, 43–52. https://doi.org/10.1016/0021-9290(91)90376-X.

(54) Nissar, A. A.; Zemanek, B.; Labatia, R.; Atkinson, D. J.; van der Ven, P. F. M.; Fürst, D. O.; Hawke, T. J. Skeletal Muscle Regeneration Is Delayed by Reduction in Xin Expression: Consequence of Impaired Satellite Cell Activation? *American Journal of Physiology-Cell Physiology* **2012**, *302* (1), C220–C227. https://doi.org/10.1152/ajpcell.00298.2011.

(55) Otten, C.; van der Ven, P. F.; Lewrenz, I.; Paul, S.; Steinhagen, A.; Busch-Nentwich, E.; Eichhorst, J.; Wiesner, B.; Stemple, D.; Strähle, U.; Fürst, D. O.; Abdelilah-Seyfried, S. Xirp Proteins Mark Injured Skeletal Muscle in Zebrafish. *PLoS ONE* **2012**, *7* (2), e31041. https://doi.org/10.1371/journal.pone.0031041.

(56) Al-Sajee, D.; Nissar, A. A.; Coleman, S. K.; Rebalka, I. A.; Chiang, A.; Wathra, R.; van der Ven, P. F. M.; Orfanos, Z.; Hawke, T. J. Xin-Deficient Mice Display Myopathy, Impaired Contractility, Attenuated Muscle Repair and Altered Satellite Cell Functionality. *Acta Physiol* **2015**, *214* (2), 248–260. https://doi.org/10.1111/apha.12455.

(57) Al-Sajee, D. Investigating the Roles of Xin Skeletal Muscle and Its Satellite Cell Population, McMaster University, 2017.

(58) Gueguen, N.; Lefaucheur, L.; Ecolan, P.; Fillaut, M.; Herpin, P. Ca2+-Activated Myosin-ATPases, Creatine and Adenylate Kinases Regulate Mitochondrial Function According to Myofibre Type in Rabbit. *The Journal of Physiology* **2005**, *564* (3), 723–735. https://doi.org/10.1113/jphysiol.2005.083030.

(59) Rudolf, R.; Mongillo, M.; Magalhães, P. J.; Pozzan, T. In Vivo Monitoring of Ca2+ Uptake into Mitochondria of Mouse Skeletal Muscle during Contraction. *Journal of Cell Biology* **2004**, *166* (4), 527–536. https://doi.org/10.1083/jcb.200403102.

(60) Gillis, J. M. Inhibition of Mitochondrial Calcium Uptake Slows down Relaxation in Mitochondria-Rich Skeletal Muscles. *Journal of Muscle Research and Cell Motility* **1997**, *18* (4), 473–483. https://doi.org/10.1023/A:1018603032590.

(61) Dorn, G. W.; Maack, C. SR and Mitochondria: Calcium Cross-Talk between Kissing Cousins. *Journal of Molecular and Cellular Cardiology* **2013**, *55*, 42–49. https://doi.org/10.1016/j.yjmcc.2012.07.015.

(62) Pernas, L.; Scorrano, L. Mito-Morphosis: Mitochondrial Fusion, Fission, and Cristae Remodeling as Key Mediators of Cellular Function. *Annu. Rev. Physiol.* **2016**, *78* (1), 505–531. https://doi.org/10.1146/annurev-physiol-021115-105011.

(63) Boncompagni, S.; Rossi, A. E.; Micaroni, M.; Beznoussenko, G. V.; Polishchuk, R. S.; Dirksen, R. T.; Protasi, F. Mitochondria Are Linked to Calcium Stores in Striated Muscle by Developmentally Regulated Tethering Structures. *MBoC* **2009**, *20* (3), 1058–1067. https://doi.org/10.1091/mbc.e08-07-0783.

(64) Merkwirth, C.; Langer, T. Mitofusin 2 Builds a Bridge between ER and Mitochondria. *Cell* **2008**, *135* (7), 1165–1167. https://doi.org/10.1016/j.cell.2008.12.005.

(65) de Brito, O. M.; Scorrano, L. Mitofusin 2 Tethers Endoplasmic Reticulum to Mitochondria. *Nature* **2008**, *456* (7222), 605–610. https://doi.org/10.1038/nature07534.

(66) Horne, J. H. Elementary Calcium-Release Units Induced by Inositol Trisphosphate. *Science* **1997**, *276* (5319), 1690–1693. https://doi.org/10.1126/science.276.5319.1690.

(67) Bononi, A.; Missiroli, S.; Poletti, F.; Suski, J. M.; Agnoletto, C.; Bonora, M.; De Marchi, E.; Giorgi, C.; Marchi, S.; Patergnani, S.; Rimessi, A.; Wieckowski, M. R.; Pinton, P. Mitochondria-Associated Membranes (MAMs) as Hotspot Ca2+ Signaling Units. In *Calcium Signaling*; Islam, Md. S., Ed.; Advances in Experimental Medicine and Biology; Springer Netherlands: Dordrecht, 2012; Vol. 740, pp 411–437. https://doi.org/10.1007/978-94-007-2888-2_17.

(68) Tatsuta, T.; Scharwey, M.; Langer, T. Mitochondrial Lipid Trafficking. *Trends in Cell Biology* **2014**, *24* (1), 44–52. https://doi.org/10.1016/j.tcb.2013.07.011.

(69) Oropesa-Nuñez, R.; Seghezza, S.; Dante, S.; Diaspro, A.; Cascella, R.; Cecchi, C.; Stefani, M.; Chiti, F.; Canale, C. Interaction of Toxic and Non-Toxic HypF-N Oligomers with Lipid Bilayers Investigated at High Resolution with Atomic Force Microscopy. *Oncotarget* **2016**, *7* (29), 44991–45004. https://doi.org/10.18632/oncotarget.10449.

(70) Sala-Vila, A.; Navarro-Lérida, I.; Sánchez-Alvarez, M.; Bosch, M.; Calvo, C.; López, J. A.; Calvo, E.; Ferguson, C.; Giacomello, M.; Serafini, A.; Scorrano, L.; Enriquez, J. A.; Balsinde, J.; Parton, R. G.; Vázquez, J.; Pol, A.; Del Pozo, M. A. Interplay between Hepatic Mitochondria-Associated Membranes, Lipid Metabolism and Caveolin-1 in Mice. *Sci Rep* **2016**, *6* (1), 27351. https://doi.org/10.1038/srep27351.

(71) Molly Gingrich. Xin as a Novel Regulator of Mitochondrial Morphology and Bioenergetics in Skeletal Muscle, McMaster University, 2018.

(72) Hamasaki, M.; Furuta, N.; Matsuda, A.; Nezu, A.; Yamamoto, A.; Fujita, N.; Oomori, H.; Noda, T.; Haraguchi, T.; Hiraoka, Y.; Amano, A.; Yoshimori, T. Autophagosomes Form at ER–Mitochondria Contact Sites. *Nature* **2013**, *495* (7441), 389–393. https://doi.org/10.1038/nature11910.

(73) Zonderland, J.; Wieringa, P.; Moroni, L. A Quantitative Method to Analyse F-Actin Distribution in Cells. *MethodsX* **2019**, *6*, 2562–2569. https://doi.org/10.1016/j.mex.2019.10.018.

(74) Dunn, K. W.; Kamocka, M. M.; McDonald, J. H. A Practical Guide to Evaluating Colocalization in Biological Microscopy. *American Journal of Physiology-Cell Physiology* **2011**, *300* (4), C723–C742. https://doi.org/10.1152/ajpcell.00462.2010.

(75) Schmid, A.; Renaud, J. F.; Fosset, M.; Meaux, J. P.; Lazdunski, M. The Nitrendipine-Sensitive Ca2+ Channel in Chick Muscle Cells and Its Appearance during Myogenesis in Vitro and in Vivo. *Journal of Biological Chemistry* **1984**, *259* (18), 11366–11372. https://doi.org/10.1016/S0021-9258(18)90870-7.

(76) Yuan, J. P.; Kiselyov, K.; Shin, D. M.; Chen, J.; Shcheynikov, N.; Kang, S. H.; Dehoff, M. H.; Schwarz, M. K.; Seeburg, P. H.; Muallem, S.; Worley, P. F. Homer Binds TRPC Family Channels and Is Required for Gating of TRPC1 by IP3 Receptors. *Cell* **2003**, *114* (6), 777–789. https://doi.org/10.1016/S0092-8674(03)00716-5.

(77) Stiber, J. A.; Tabatabaei, N.; Hawkins, A. F.; Hawke, T.; Worley, P. F.; Williams, R. S.; Rosenberg, P. Homer Modulates NFAT-Dependent Signaling during Muscle Differentiation. *Developmental Biology* **2005**, *287* (2), 213–224. https://doi.org/10.1016/j.ydbio.2005.06.030.

(78) Sin, J.; Andres, A. M.; Taylor, D. J. R.; Weston, T.; Hiraumi, Y.; Stotland, A.; Kim, B. J.; Huang, C.; Doran, K. S.; Gottlieb, R. A. Mitophagy Is Required for Mitochondrial Biogenesis and Myogenic Differentiation of C2C12 Myoblasts. *Autophagy* **2016**, *12* (2), 369–380. https://doi.org/10.1080/15548627.2015.1115172.

(79) Johannsen, D. L.; Ravussin, E. The Role of Mitochondria in Health and Disease. *Current Opinion in Pharmacology* **2009**, *9* (6), 780–786. https://doi.org/10.1016/j.coph.2009.09.002.

(80) Luft, R.; Ikkos, D.; Palmieri, G.; Ernster, L.; Afzelius, B. A CASE OF SEVERE HYPERMETABOLISM OF NONTHYROID ORIGIN WITH A DEFECT IN THE MAINTENANCE OF MITOCHONDRIAL RESPIRATORY CONTROL: A CORRELATED CLINICAL, BIOCHEMICAL, AND MORPHOLOGICAL STUDY. *J. Clin. Invest.* **1962**, *41* (9), 1776–1804. https://doi.org/10.1172/JCI104637.

(81) Szabadkai, G.; Bianchi, K.; Várnai, P.; De Stefani, D.; Wieckowski, M. R.; Cavagna, D.; Nagy, A. I.; Balla, T.; Rizzuto, R. Chaperone-Mediated Coupling of Endoplasmic Reticulum and

Mitochondrial Ca2+ Channels. *Journal of Cell Biology* **2006**, *175* (6), 901–911. https://doi.org/10.1083/jcb.200608073.

(82) Naon, D.; Zaninello, M.; Giacomello, M.; Varanita, T.; Grespi, F.; Lakshminaranayan, S.; Serafini, A.; Semenzato, M.; Herkenne, S.; Hernández-Alvarez, M. I.; Zorzano, A.; De Stefani, D.; Dorn, G. W.; Scorrano, L. Critical Reappraisal Confirms That Mitofusin 2 Is an Endoplasmic Reticulum–Mitochondria Tether. *Proc Natl Acad Sci USA* **2016**, *113* (40), 11249–11254. https://doi.org/10.1073/pnas.1606786113.

(83) Holt, I.; Fuller, H. R.; Schindler, R. F. R.; Shirran, S. L.; Brand, T.; Morris, G. E. An Interaction of Heart Disease-Associated Proteins POPDC1/2 with XIRP1 in Transverse Tubules and Intercalated Discs. *BMC Mol and Cell Biol* **2020**, *21* (1), 88. https://doi.org/10.1186/s12860-020-00329-3.

(84) Galbiati, F.; Engelman, J. A.; Volonte, D.; Zhang, X. L.; Minetti, C.; Li, M.; Hou, H.; Kneitz, B.; Edelmann, W.; Lisanti, M. P. Caveolin-3 Null Mice Show a Loss of Caveolae, Changes in the Microdomain Distribution of the Dystrophin-Glycoprotein Complex, and T-Tubule Abnormalities. *Journal of Biological Chemistry* **2001**, *276* (24), 21425–21433. https://doi.org/10.1074/jbc.M100828200.

(85) Volonte, D.; McTiernan, C. F.; Drab, M.; Kasper, M.; Galbiati, F. Caveolin-1 and Caveolin-3 Form Heterooligomeric Complexes in Atrial Cardiac Myocytes That Are Required for Doxorubicin-Induced Apoptosis. *American Journal of Physiology-Heart and Circulatory Physiology* **2008**, *294* (1), H392–H401. https://doi.org/10.1152/ajpheart.01039.2007.

(86) Alazami, A. M.; Patel, N.; Shamseldin, H. E.; Anazi, S.; Al-Dosari, M. S.; Alzahrani, F.; Hijazi, H.; Alshammari, M.; Aldahmesh, M. A.; Salih, M. A.; Faqeih, E.; Alhashem, A.; Bashiri, F. A.; Al-Owain, M.; Kentab, A. Y.; Sogaty, S.; Al Tala, S.; Temsah, M.-H.; Tulbah, M.; Aljelaify, R. F.; Alshahwan, S. A.; Seidahmed, M. Z.; Alhadid, A. A.; Aldhalaan, H.; AlQallaf, F.; Kurdi, W.; Alfadhel, M.; Babay, Z.; Alsogheer, M.; Kaya, N.; Al-Hassnan, Z. N.; Abdel-Salam, G. M. H.; Al-Sannaa, N.; Al Mutairi, F.; El Khashab, H. Y.; Bohlega, S.; Jia, X.; Nguyen, H. C.; Hammami, R.; Adly, N.; Mohamed, J. Y.; Abdulwahab, F.; Ibrahim, N.; Naim, E. A.; Al-Younes, B.; Meyer, B. F.; Hashem, M.; Shaheen, R.; Xiong, Y.; Abouelhoda, M.; Aldeeri, A. A.; Monies, D. M.; Alkuraya, F. S. Accelerating Novel Candidate Gene Discovery in Neurogenetic Disorders via Whole-Exome Sequencing of Prescreened Multiplex Consanguineous Families. *Cell Reports* **2015**, *10* (2), 148–161. https://doi.org/10.1016/j.celrep.2014.12.015.

(87) Ashton, K. J.; Tupicoff, A.; Williams-Pritchard, G.; Kiessling, C. J.; See Hoe, L. E.; Headrick, J. P.; Peart, J. N. Unique Transcriptional Profile of Sustained Ligand-Activated Preconditioning in Pre- and Post-Ischemic Myocardium. *PLoS ONE* **2013**, *8* (8), e72278. https://doi.org/10.1371/journal.pone.0072278.